On the Migrating Speed of Free Alternate Bars

Michihide Ishihara

Doctoral Program in Environmental Science and Technology

Graduate School of Science and Technology

Niigata University

Table of Contents

1 Introduction

1.1 Background and purpose of this study

Periodic forms can spontaneously occur along the surface of a river channel bed. These forms are called riverbed waves because of their geometrical shapes and physical properties. Riverbed waves can be classified as small-scale, mesoscale, and large-scale, depending on the spatial scales, which include the wavelength and wave height [1]. Small-scale riverbed waves have wavelengths on the scale of the water depth, whereas mesoscale riverbed waves have wavelengths on the river width scale and wave heights on the water depth scale. Large-scale riverbed waves have larger scales. The target of this study was the alternate bars that correspond to mesoscale riverbed waves. Alternate bars are riverbed waves that are spontaneously formed in rivers and are located at sites from the alluvial fan to the natural embankment. When observing alternate bars from the sky using aerial photographs (Fig. 1.1(a)), the tip part is diagonally connected to the left and right riverbanks; a deep-water pool is located downstream of this tip. Alternate bars can be broadly classified into two categories: 1) free bars, which occur naturally in straight channels owing to the instability of the bottom surface, and 2) forced bars, which occur because of forcing derived from the channel's planar shape and boundary conditions [1]. In this study, among the above categories, free alternate bars are targeted. Because of the physical properties of these alternate bars, their phases are changed in a similar manner to water surface waves during floods of a magnitude that causes active sediment transport (Fig. 1.1(a),(b)).

Over the years, numerous studies have been conducted on alternate bars. One of the initial studies consisted of flume experiments that were performed by Kinoshita [2]. Kinoshita conducted long-term flume experiments to understand the dynamics of alternate bars that can produce meandering streams. He reported that 1) alternate bars have a globally uniform migrating speed and wavelength, 2) alternate bars in the early stages of development have short wavelengths and fast migrating speeds, and 3) the migrating

speed becomes slower with the growth of wavelengths. These results have been confirmed in subsequent studies [3, 4, 5, 6]. In addition to the aforementioned conclusions, a formula was proposed to calculate the migrating speed of alternate bars based on experimental results, with the Froude number and shear velocity as the dominant physical quantities. However, the validity of this formula was not demonstrated in the same study.

In addition to studies using flume experiments, several studies have applied mathematical analyses to understand the mechanism of development of alternate bars. The first mathematical study on alternate bars was conducted by Callander [7], who extended the instability analysis proposed by Kennedy [8] for small-scale bed waves to a two-dimensional plane problem, and theoretically discussed the physical quantities that govern the generation of mesoscale riverbed waves. This study led to a unified study on the generation mechanism of small-scale and meso-scale riverbed waves using instability analysis with the introduction of a lag distance [9, 10]. After that, studies aimed at predicting the conditions for the occurrence of alternate bars and the wavelength and wave height after their development have been conducted [11, 12, 13, 14, 15, 16, 17]. In these instability analyses, an equation for calculating the migrating speed of small bed perturbation was derived during analysis. Kuroki and Kishi[11] compared the calculated and measured values of the migrating speed and reported that the calculated value reproduced the measured value well. The calculated value is the migrating speed at the wavenumber of the maximum amplification rate, and the measured value is calculated from the time variation of the position of the tip of the bar. However, because the migrating speed obtained from the analysis corresponds to the wave number, its spatial distribution has neither been calculated nor determined from measurements.

With the emergence of instability analysis, numerical analyses of riverbed fluctuations during the occurrence and development of alternate bars began. Shimizu [18] reported for the first time that numerical analysis can satisfactorily reproduce each process of the occurrence and development of alternate bars. Recently, Federici [19] reported the propagation direction of small-bed perturbation by performing instability and numerical

analyses.

Other studies using flume experiments [20, 21, 22, 23, 24, 25, 26] have investigated the effects of external factors, such as the amount of sediment supply and flow discharge, on the dynamics of alternate bars. Crosato et al.[23, 24] reported that alternate bars eventually shift from being migrating bars to steady bars; they performed flume experiments and a numerical analysis to verify this. Next, Venditti et al. [25] reported that when sediment supply was interrupted after alternate bars occurred, the bed slope and Shields number decreased, and the bars disappeared accordingly. Podolak et al. [26] studied the response of alternate bars to sediment supply by increasing the sediment supply during the occurrence and development of alternate bars. A non-migrating bar changed to a migrating bar with an increase in the bed slope and Shields number because of the increase in the sediment supply. This result from Podolak et al. was followed up in a subsequent study [28].

Several studies have also been conducted on real rivers [29, 30]. Eekhout et al. [29] investigated the dynamics of alternate bars in rivers for nearly three years and reported that the migrating speed decreased as the wavelength and wave height of alternate bars increased and the bed slope decreased. In addition, Adami et al.[30] studied the behavior of alternate bars in the Alps and Rhine River over several decades. They established the relationship between the flow discharge and migrating speed of bars and confirmed that bars move less when the flow rate is very high and move significantly when the flow discharge is in the middle scale of the flow discharge.

Through previous studies, predicting the occurrence and geometry of alternate bars has become possible to some extent. In contrast, an understanding of the nature of the migrating speed of alternate bars is still lacking. In this study, considering the physics of alternate bars, which has not yet been fully demonstrated, we focused on the migrating speed and conducted the following experiments to clarify the dominant physical quantities, and the existence and scale of their spatial distribution and migrating speed.

1.2 Hydraulic Phenomena Targeted in This Study

1.2.1 Migrating Phenomena of Alternating Bars in Flume Experiments

One of the reasons for the lack of clarity in the spatial distribution of the migrating speed of alternate bars and their dominant physical quantity is that the technology to measure the migrating phenomenon of alternate bars and the hydraulic quantity above them with high spatial resolution has not yet been developed. In many previous studies using flume experiments, the measurement of the bed shape was done by interrupting the flow of water, and it was not possible to simultaneously measure the bed shape, which continues to deform as the bar develops, and the basic hydraulic quantities such as water depth and flow velocity above it. In addition, even if it is possible to measure the hydraulic quantities on the bed and on the top of the bed in the water, it is not possible to quantify the migrating phenomenon of the alternate bars, which changes from time to time, because the data is only spatially low resolution. This problem was also observed in actual rivers. The spatial distribution of the migrating speed of the alternate bars and their dominant physical quantity are difficult to be clarified from the measured data. To the best of the authors' knowledge, no numerical analysis or mathematical model has been developed to quantify the spatial distribution of the migrating speed, and even if such a method existed, its validity would remain qualitative due to the lack of measured data.

In recent years, Stream Tomography (ST) has been developed to simultaneously measure the geometrical shape of the water surface and bed while keeping the water flowing, albeit on a flume experimental scale [33]. It is now possible to quantify the development and propagation of alternate bars and the hydraulic quantities on them using ST measurements [34]. This allows us to discuss the spatial distribution of the migrating speed of alternate bars and their dominant physical quantities from the ST measurements, as well as to discuss validations of the numerical analysis and the mathematical model for calculating the migrating speed.

First, the author discussed the existence of the spatial distribution of the migrating speed of the alternate bars based on the measurements of ST in the flume experiment. Next, the theoretical equation was derived to quantify the spatial distribution of the migrating speed of the alternate bars and to understand the dominant physical quantity of the migrating speed, and the validity of the equation was verified based on ST measurements. The validity of the equation was verified based on ST measurements.

1.2.2 Migrating Phenomena of Alternating Bars in Actual Rivers

The theoretical equation proposed by the author is intended to understand and predict the migrating phenomena of alternate bars in real rivers. Therefore, it is necessary to verify the validity of the theoretical equation not only in flume experiments but also in real rivers with completely different sizes, riverbed materials, and hydraulic conditions. In this study, the validity of the author's theoretical equation is examined in a real river where an alternate bars has been moved by a flood.

The actual river in this study is the Chikuma River, which flows through Nagano Prefecture, Japan. It is the longest river in Japan, with a channel length of 300 km. This river experienced large-scale shifting of alternate bars in the river channel due to runoff associated with Typhoon No. 19 in October 2019. We reproduced the outflow condition by hydraulic analysis, and calculated the migrating speed using the theoretical equation proposed by the author based on the hydraulic quantity obtained from the analysis. By comparing the calculated migrating speed with the measured one, we verified whether the theoretical equation is valid for the actual river.

1.3 Academic Importance of This Study

1.3.1 Demonstration of the Validity of Pseudo-Fixed Beds

As shown in Section 1.1, meso-scale river-bed waves, such as those on alternate bars, behave in a way that can be regarded as a wave phenomenon during floods in actual

rivers and during water flow in flume experiments. In addition, previous studies[1, 35] have suggested that the time scale of the process of generation and development of riverbed waves is sufficiently slow compared to the flow in the river. However, this has not yet been demonstrated. Therefore, the quantification of the migrating speed of riverbed waves itself is of great academic importance.

In addition, mathematical analyses and measurements of riverbed waves have been conducted under the assumption of a moving bed, where the bed height increases or decreases. If the migrating speed of riverbed waves can be clarified, and it can be demonstrated that the physics of riverbed waves can be treated as pseudo-fixed beds; a fixed bed where the bed height does not change, it can be expected that mathematical analysis and measurement will be freed from the limitations derived from the assumption of a moving bed.

In particular, the measurement principle can be adapted to the time scale of the process of generation and development of riverbed waves by relaxing the restriction of the time interval of measurement.

1.3.2 Demonstration of the Validity of Previous Mathematical Analyses

The occurrence and development of alternate bars is a physical phenomenon on the riverbed in flowing water, and it has been difficult to quantify their occurrence and development processes. In previous studies, the occurrence and development processes of alternate bars have been estimated by mathematical methods. Intability analysis has been used since the late 1960s to estimate the occurrence conditions, equilibrium wave height, and equilibrium wavelength of meso-scale riverbed waves, including alternate bars. The most important contribution of instability analysis to the understanding of the physics of alternate bars is the clarification of the occurrence conditions. The instability analysis has been applied to various conditions of riverbed wave occurrence and its effectiveness has been well demonstrated. The instability analysis can also estimate the migrating

speed for each wave number. However, it has not been clarified what the migrating speed obtained from the instability analysis corresponds to in real phenomenon.

If the spatial distribution of the migrating speed of the alternate bars is clarified by this study, it is highly possible to clarify what the migrating speed obtained from the instability analysis corresponds to in the real phenomenon. In addition, it is highly possible to show the validity of the assumption of quasi-steady flow applied in the instability analysis. In addition to the above, it is expected that the researches [36], which proposed a unified classification of three riverbed waves based on wave theory assuming a fixed bed, and [37], which estimated the geometric shape of the bed from the minute amplitude of the water surface by data-driven analysis, will be sufficiently validated.

1.4 Engineering Importance of This Study

In recent years, river banks and embankments have been frequently damaged by floods, regardless of the size of the river. In the floods caused by Typhoon No. 19 in the first year of 2021, a railroad bridge fell due to a levee failure at Suwagata (Fig. 1.2) and a levee break caused flooding at Hoyasu. In the most recent flood caused by heavy rain in August 2021, a levee failure occurred at Kamiozuma on the Sai River.

The three main types of damage caused by levee failures and breaches are overtopping, erosion/scouring, and seepage/piping. The Suwagata site of the Chikuma River is estimated to be of the erosion/scouring type, while the Hoyasu site is of the overflow type[38]. In addition, the Kamiozuma site of the Sai River is estimated to be of the erosion/scouring type based on the trace water level at the time of discharge and the damage. These are representative damage cases of rivers managed by the national government, and the number of cases will increase if rivers managed by prefectures are included.

Alternate bars, which are the subject of this study, are considered to have a strong influence on erosion/scouring type damage patterns. Alternate bars have a wavelength of the river width scale and a wave height of the water depth scale, and are considered to

eccentric the flood flow along the bank. It is thought that the alternate bars form water colliding front to induce riverbank erosion and local scouring, leading to erosion and scouring type embankment damage. The location of the water colliding front changes with each flood event due to the migration of the alternate bars.

Two main measures are used for the above: revetment and foundation root insertion. According to Guide[39] to River Channel Planning, the migration of bars should be taken into account when setting the section of revetment and the depth of foundation root embankment. However, the physics of alternate bars is still unclear, and the methods for estimating the migrating speed and distance of bars have not yet been established. For example, in the straight section of the river channel classified as Segment 1, bars are considered to migrate and revetments and foundation roots are set to be constructed uniformly throughout the section. However, despite the straight section of the river channel at Suwagata in Chikuma River, the bar had stopped migration more than ten years before the outflow of water by Typhoon No. 19 in 2019. The bars in the section before and after this point was migrated by about 600 m due to the outflow of the same typhoon, resulting in an embankment loss of about 300 m and the fall of the Ueda Electric Railway bridge. If the method for estimating the migration of bars can be established, effective preventive measures against such damage can be formulated.

1.5 Structure of This Study

This study is composed of seven chapters.

In Section 1, we first presented the background and purpose of the study, and summarized the lack of understanding of alternate bars migration, especially the spatial distribution of migrating speed and their dominant hydraulic quantities. Next, the target phenomenon was described. Finally, the academic and engineering importance of this study was presented.

In Section 2, we described flume experiments using a device (ST) that can measure

the geometric shapes of the water surface and bed simultaneously and with high spatial resolution. Specifically, flume experiments was conducted under the hydraulic conditions where alternate bars occur, and the spatial distribution of the migrating speed of the alternate bars was discussed based on the time variation of the bed shape measured by the ST and the wave theory.

In Section 3, in order to quantify the spatial distribution of the migrating speed of the alternate bars, the HPDE for the bed level was derived, assuming that the alternate bars can be regarded as a wave phenomenon. Specifically, the HPDE for the bed level was derived by mathematically transforming the four equations that are the governing equations in general river bed fluctuation analysis: the flow continuity equation, the equation of motion, the continuity equation of bed, and the bedload function. By formulating the advection velocity given to the advection term of the equation, an equation for calculating the migrating speed of alternate bars was derived.

In Section 4, the validity of the equation derived in Section 3 was verified based on the properties of the HPDE for the bed level and the measurements obtained in Section 2. By discretizing the equation using the difference method and integrating it numerically, the riverbed variation amount per time can be calculated. In this study, the temporal change of the bed shape was measured by ST, so the measured riverbed variation amount can be obtained from the same data. Therefore, the validity of the equation derived in Section 3 was verified by comparing the changes in the riverbed variation amount in both cases.

In Section 5, we quantified and discussed whether the migrating speed of the alternate bars shown in Section 2 has a spatial distribution, using the formula for calculating the migrating speed verified in Section 3.

In Section 6, we verified the validity of the proposed method for calculating migration speed in actual rivers with completely different sizes, bed materials, and hydraulic conditions.

In Section 7, we summarized the main research results of each section.

2 Quantification of the Propagation Phenomenon in Alternate Bars Based on the Flume Experiment

As mentioned in Section 1.2.1 of the previous section, one of the reasons why the spatial distribution of the migrating speed of alternate bars and their dominant physical quantity are not clear is the lack of technology to measure the migation phenomenon of alternate bars and the hydraulic quantity on them with high spatial resolution. In this study, we measured the geometric shapes of the water surface and the bed of the alternate bars during its development and migration in flume experiments simultaneously with high spatial resolution. In this section, the outline of the flume experiments was described.

2.1 Experimental Setup

Figure 2.1 shows a plan view of the experiment flume. The experimental channel consisted of a flume channel with a straight rectangular cross section. The flume had a length of 12.0 m, width of 0.45 m, and depth of 0.15 m. Fixed weirs with the same width as the flume were located 2.7 m from the upstream and downstream ends of the flume. Over the section 2.7–9.3 m from the upstream end that was sandwiched by these weirs, the initial bed of the channel for the experiment was a set flat bed. The bed was fabricated from a non-cohesive material with a mean diameter of 0.76 mm and the bed thickness was 5.0 cm.

For water supply to the channel, circulation-type pumping from a water tank at the downstream end to a water tank at the upstream end was adopted; water was steadily supplied. The accuracy of the water discharge was confirmed using an electromagnetic flowmeter.

2.2 Experimental Condition

The purpose of this study is to understand the dominant physical quantities of the migrating speed of the alternate bars and the existence and scale of their spatial distribution. In the following experiment, we set up the hydraulic conditions under which alternate bars are expected to develop and migrate. It has been theoretically shown that the occurrence of alternate bars can be estimated using the river width–depth ratio [7, 11]. Kuroki [11] showed that the type of bars occurred can be classified based on $BI_0^{0.2}/h_0$, which is the bed slope I_0 added to the river width-depth ratio β. In this study, we set two conditions that correspond to the area of occurrence of alternate bars, as shown in Table. 2.1.

The validity of the formula was verified by comparing the calculated values of the migrating speed of the instability analysis and the calculated values of the migrating speed derived in this study. Therefore, based on the characteristics of instability analysis, the conditions were set such that the particle size and Shields number were fixed, and the river width–depth ratio became a variable. The same experiment was conducted twice for each condition to confirm the reproducibility of the results.

These experimental conditions exceed the critical Shields number of 0.034 obtained from equation of Iwagaki [31]. The sediment supply condition at the upstream end was set to no supply. The no-supply condition was chosen because preliminary experiments comparing the effects of the presence and absence of sediment supply on the spatial distribution of the migrating speed of alternate bars and its temporal variation showed that the spatial distribution of the migrating speed was more likely to expand in the no-supply condition.

Water flow was carried out for 2 h during this experiment with the aforementioned conditions. At this time, alternate bars developed, and their propagation and shape change became slow.

2.3 Measurement Method for the Bed Surface and Water Surface

In this study, we used Stream Tomography (ST), which was developed by Hoshino [33], to measure the bed and water levels in a plane while the water was flowing. In this study, the aforementioned measurements were performed with a spatial resolution of 2 cm^2 for every minute. The water depth was calculated from the difference between the water level and bed level. Because the ST measurements were missing near the side walls, the data of 0.38-m width excluding the side walls were used.

2.4 Measurement Results

In this section, we describe the migration phenomena of alternate bars based on high-resolution spatial measurements by the ST, using a plan view of the basal level of Fig. 2.2 and a longitudinal section of Fig. 2.3. The same figures show the measurement results of Condition 2, where typical alternate bars were formed. The results of the other condition differed from those of Condition 2 only in terms of the wavelength and wave height, but no essential difference was observed. For the results of the other condition, please refer to the database [32].

Figure 2.2 shows the plan view of the deviation of the bed level by ST. The origin of the vertical coordinates of the ST is the flume bottom. Therefore, the water level and bed level represent the height from the bed of the flume. In this study, the initial bed was shaped to be completely flat in the transverse direction as much as possible, but the bed was not completely flat due to the limitation of the shaping jig. The transverse slope of the initial bed may affect the occurrence and development of alternate bars. However, the experimental results shown in Fig. 2.2 are almost the same as the equilibrium wave height and wavelength obtained by the instability analysis described in Section 7.4 of the Discussion. In addition, the alternate bars occurred and developed were almost identical

to the geometrical shapes of alternate bars in previous studies [2, 19, 23, 25, 26]. These results suggest that the transverse slope of the initial riverbed is not a concern.

First, it can be observed that the bottom shape did not change much from the initial flat bed in Fig. 2.2 from (a) to (d). Second, the bed topography in which deposition and scouring are alternately repeated in the downstream direction, that is, 2.0 m, 3.0 m, and 5.0 m from the upstream end, can be observed; thus, it can be confirmed that alternate bars occurred (Fig. 2.2(e)). In this study, we defined (e) 40 min, in which the geometric features of the alternate bars were confirmed from the measured result by the ST, as the occurrence time of the alternate bars. The alternate bars develop undulations with time, becoming more sedimented in the sedimented areas and more scoured in the scoured areas, which indicates that the entire bar is gradually migrating downstream. A series of observations from (g) 60 min to (m) 120 min of water flow shows that bars are migrating at a constant speed.

Next, Figure 2.3 shows the longitudinal distribution of the deviation in the bed level on the green dotted line in Fig. 2.2. Figure 2.3 shows (a) the initial stage of the experiment, (b) the occurrence of alternate bars, (c) the intermediate stage of the experiment, and (d) the final stage of the experiment. Figure 2.3 shows three results, where each one is 10 min apart. First, the deviation of the bed level was confirmed to maintain a nearly flat bed from 1 min to 20 min (Fig. 2.3(a)). After (b) 60 min, three bed undulations developed 2.5 m, 4.5 m, and 5.5 m from the upstream end. The amplitudes of the bed undulations developed, and they migrated in the downstream direction. This undulation migrated downstream with amplification of wave height from (b) 60 to 120 min of water flow. The above results indicate that the waviness of the alternate bars is being measured. In Fig. 2.3(d), a decrease in the bed level was observed in the upstream section because the experimental conditions were set to no sediment supply. On the other hand, there was no decrease in the bed level in the downstream of the half of the channel even at the time when the water flow was terminated. This suggests that the effect of the no-sediment supply condition did not spread downstream of the half of the channel at the end of the

experiment.

The linear wave theory indicates that the phase propagates without deforming the waveform if a wave propagates with a spatial and temporal constant migrating speed. Conversely, in nonlinear wave theory, in which the migrating speed has a spatial distribution and temporal changes, the wave propagates with deformation of the waveform. From the viewpoint of the aforementioned wave theories, the migrating speed of the bars after the occurrence of alternate bars in (b) has a spatial distribution and is estimated to change with time, and it has the characteristics of a nonlinear wave.

2.5 Conclusion of Section 2

In this section, Flume experiments were conducted under the hydraulic conditions in which alternate bars develop and migrate, and the shapes of the bed and water surface, which change from time to time during the flowing of water, were measured simultaneously by ST. From the results of the above measurements, it was confirmed that the alternate bars migrate while changing its shape. The results were discussed based on the wave theory, and it was found that the alternate bars have a nonlinear wave property in that its migrating speed have a spatial distribution and changes with time. This suggests that the migrating speed of the alternate bars have a spatial distribution.

3 Derivation of the Calculation Formula for the Migrating Speed of Alternate Bars

3.1 Derivation of the hyperbolic partial differential equation for the bed lebel

As shown in the previous section, the measurement results of this study show the nature of the wave in the process of the occurrence and development of alternate bars. These findings are similar to what has been reported in the literature [2, 19, 23, 25, 26]. In other words, there is scope for quantifying the spatial distribution of the migrating speed by an indirect method using a mathematical model such as the HPDE [5], which is suitable for describing the wave phenomena. The formula for calculating the migrating speed is also derived from instability analysis [7, 11]. However, because the formula calculates the migrating speed for each wave number, the spatial distribution of the migrating speed cannot be quantified. Another possible method is to set up feature points at the front edge of an alternate bar and to calculate the migrating speed based on the trajectory. However, both methods fail to obtain a continuous spatial distribution of the migrating speed. In addition, it is not possible to calculate the migrating speed using numerical analysis of the occurrence and development of bars. Therefore, in this study, we derived a hyperbolic partial differential equation for the bed level and quantified the spatial distribution of the migrating speed of alternate bars using the advection velocity, which is the coefficient of the advection term of the HPDE.

This section describes the derivation process of the HPDE for bed level z. In addition, four different formulas were obtained depending on the physical assumptions. This includes whether the dimension is one-dimensional or two-dimensional, and whether the flow is stationary or unsteady. First, regarding the stationarity of flow, as we confirmed that the non-stationary state in the phenomenon targeted by this study is very small from the verification results described in Appendix A, we decided to consider only the

stationary state. In terms of dimensions, the geometric shape of the alternate bars and the flow each have two-dimensional plane characteristics. Therefore, we aimed to derive a two-dimensional stationary equation.

The derivation of the HPDE for the bed level can be used for the continuous equation of the sediment, sediment functions, and the equation of the water surface profile. For the derivation, the Exner equation was used as the continuous equation of the sediment, and the Meyer–Peter and Müller (MPM) formula were used as the sediment function and two-dimensional equation of the water surface profile, respectively. The application of the HPDE to the various sediment functions was examined using the method described in the next section. In this study, the MPM formula, which is simple and has good applicability, was adopted. Vectors for longitudinal Eq. (3.2) and transverse Eq. (3.3) for the sediment flux were assumed based on equation of Watanabe [40]. Equation (3.7) was used to calculate the Shields number. We derived the steady two-dimensional equation of the water surface profile (Eq. (3.5), Eq. (3.6)) to derive the HPDE for the bed level. For details on the derivation process of the steady two-dimensional equation for the water surface profile, please refer to Appendix B.

$$\frac{\partial z}{\partial t} + \frac{1}{1-\lambda}\left(\frac{\partial q_{Bx}}{\partial x} + \frac{\partial q_{By}}{\partial y}\right) = 0 \tag{3.1}$$

$$q_{Bx} = 8\left(\tau_* - \tau_{*c}\right)^{3/2}\sqrt{sgd^3}\left(\frac{u}{V} - \frac{\gamma^{'}}{\tau_*^{1/2}}\frac{\partial z}{\partial x}\right) \tag{3.2}$$

$$q_{By} = 8\left(\tau_* - \tau_{*c}\right)^{3/2}\sqrt{sgd^3}\left(\frac{v}{V} - \frac{\gamma^{'}}{\tau_*^{1/2}}\frac{\partial z}{\partial y}\right) \tag{3.3}$$

$$\gamma^{'} = \sqrt{\frac{\tau_{*c}}{\mu_s \mu_k}} \tag{3.4}$$

$$\frac{\partial h}{\partial x} = -\frac{\partial z}{\partial x} - I_{ex} - \frac{3}{5}\frac{u^2}{gI_{ex}}\frac{\partial I_{ex}}{\partial x} + \frac{3}{10}\frac{u^2}{gI_e}\frac{\partial I_e}{\partial x} + \frac{2}{5}\frac{uv}{gI_{ey}}\frac{\partial I_{ey}}{\partial y} + \frac{3}{10}\frac{uv}{gI_e}\frac{\partial I_e}{\partial y} - \frac{uv}{gI_{ex}}\frac{\partial I_{ex}}{\partial y} \quad (3.5)$$

$$\frac{\partial h}{\partial y} = -\frac{\partial z}{\partial y} - I_{ey} - \frac{3}{5}\frac{v^2}{gI_{ey}}\frac{\partial I_{ey}}{\partial y} + \frac{3}{10}\frac{v^2}{gI_e}\frac{\partial I_e}{\partial y} + \frac{2}{5}\frac{uv}{gI_{ex}}\frac{\partial I_{ex}}{\partial x} + \frac{3}{10}\frac{uv}{gI_e}\frac{\partial I_e}{\partial x} - \frac{uv}{gI_{ey}}\frac{\partial I_{ey}}{\partial x} \quad (3.6)$$

$$\tau_* = \frac{hI_e}{sd} \quad (3.7)$$

where z is the bed level, t is the time, λ is the porosity of the bed, q_{Bx} is the longitudinal sediment flux, x is the distance of the longitudinal direction, q_{By} is the transverse sediment flux, y is the distance of the transverse direction, τ_* is the composite Shields number, τ_{*c} is the critical Shields number, s is the specific gravity of sediments in water, g is the acceleration due to gravity, d is the sediment size, u is the longitudinal flow velocity, V is the composite flow velocity, v is the transverse flow velocity, μ_s is the coefficient of static friction, μ_s is the coefficient of dynamic friction, and h is the depth. In addition, $I_{bx} = -\partial z/\partial x$ is the longitudinal bed slope, I_{ex} is the longitudinal energy slope, $I_{by} = -\partial z/\partial y$ is the transverse bed slope, and I_{ey} is the transverse energy slope.

First, by applying the chain rule of differentiation to $\partial q_{Bx}/\partial x$ in Eq. (3.1), we can obtain the following, where n is the coefficient of roughness.

$$\begin{aligned}
\frac{\partial q_{Bx}}{\partial x} &= \frac{\partial q_{Bx}}{\partial \tau_*}\frac{\partial \tau_*}{\partial x} + \frac{\partial q_{Bx}}{\partial u}\frac{\partial u}{\partial x} + \frac{\partial q_{Bx}}{\partial V}\frac{\partial V}{\partial x} + \frac{\partial q_{Bx}}{\partial(\partial z/\partial x)}\frac{\partial(\partial z/\partial x)}{\partial x} \\
&= \frac{\partial q_{Bx}}{\partial \tau_*}\left(\frac{\partial \tau_*}{\partial h}\frac{\partial h}{\partial x} + \frac{\partial \tau_*}{\partial I_e}\frac{\partial I_e}{\partial x}\right) + \frac{\partial q_{Bx}}{\partial u}\frac{\partial u}{\partial x} + \frac{\partial q_{Bx}}{\partial V}\frac{\partial V}{\partial x} + \frac{\partial q_{Bx}}{\partial(\partial z/\partial x)}\frac{\partial^2 z}{\partial x^2} \\
&= \frac{\partial q_{Bx}}{\partial \tau_*}\left(\frac{I_e}{sd}\frac{\partial h}{\partial x} + \frac{h}{sd}\frac{\partial I_e}{\partial x}\right) + \frac{\partial q_{Bx}}{\partial u}\frac{\partial u}{\partial x} + \frac{\partial q_{Bx}}{\partial V}\frac{\partial V}{\partial x} + \frac{\partial q_{Bx}}{\partial(\partial z/\partial x)}\frac{\partial^2 z}{\partial x^2} \\
&= \frac{\partial q_{Bx}}{\partial \tau_*}\frac{I_e}{sd}\left(\frac{\partial h}{\partial x} + \frac{h}{I_e}\frac{\partial I_e}{\partial x}\right) + \frac{\partial q_{Bx}}{\partial u}\frac{\partial u}{\partial x} + \frac{\partial q_{Bx}}{\partial V}\frac{\partial V}{\partial x} + \frac{\partial q_{Bx}}{\partial(\partial z/\partial x)}\frac{\partial^2 z}{\partial x^2}
\end{aligned} \quad (3.8)$$

In addition, $\partial I_e/\partial x$ in Eq. (3.8) becomes the following when the chain rule is applied to

differentiate the Manning flow velocity Eq. (3.9).

$$V = \frac{1}{n} {I_e}^{1/2} h^{2/3} \tag{3.9}$$

$$\frac{\partial I_e}{\partial x} = \frac{\partial I_e}{\partial h}\frac{\partial h}{\partial x} + \frac{\partial I_e}{\partial V}\frac{\partial V}{\partial x} = -\frac{4}{3}\frac{I_e}{h}\frac{\partial h}{\partial x} + 2\frac{I_e}{V}\frac{\partial V}{\partial x} \tag{3.10}$$

Substituting Eq. (3.10) in Eq. (3.8) and rearranging, we can obtain the following equation.

$$\frac{\partial q_{Bx}}{\partial x} = \frac{\partial q_{Bx}}{\partial \tau_*}\frac{I_e}{sd}\left(-\frac{1}{3}\frac{\partial h}{\partial x} + 2\frac{h}{V}\frac{\partial V}{\partial x}\right) + \frac{\partial q_{Bx}}{\partial u}\frac{\partial u}{\partial x} + \frac{\partial q_{Bx}}{\partial V}\frac{\partial V}{\partial x} + \frac{\partial q_{Bx}}{\partial (\partial z/\partial x)}\frac{\partial^2 z}{\partial x^2} \tag{3.11}$$

$\partial q_{Bx}/\partial \tau_*$, $\partial q_{Bx}/\partial u$, $\partial q_{Bx}/\partial V$, $\partial q_{Bx}/\partial(\partial z/\partial x)$ in the aforementioned equation is given as follows.

$$\frac{\partial q_{Bx}}{\partial \tau_*} = 8\left(\tau_* - \tau_{*c}\right)^{1/2}\sqrt{sgd^3}\frac{3}{2}\left[\frac{u}{V} - \frac{\gamma^{'}}{\tau_*^{1/2}}\left\{1 - \frac{1}{3\tau_*}\left(\tau_* - \tau_{*c}\right)\right\}\frac{\partial z}{\partial x}\right] \tag{3.12}$$

$$\frac{\partial q_{Bx}}{\partial u} = 8\left(\tau_* - \tau_{*c}\right)^{3/2}\sqrt{sgd^3}\frac{1}{V} \tag{3.13}$$

$$\frac{\partial q_{Bx}}{\partial V} = -8\left(\tau_* - \tau_{*c}\right)^{3/2}\sqrt{sgd^3}\frac{u}{V^2} \tag{3.14}$$

$$\frac{\partial q_{Bx}}{\partial (\partial z/\partial x)} = -8\left(\tau_* - \tau_{*c}\right)^{3/2}\sqrt{sgd^3}\frac{\gamma^{'}}{\tau_*^{1/2}} \tag{3.15}$$

Equation (3.5) is used for $\partial h/\partial x$. Substituting Eq. (3.5), Eq. (3.12), Eq. (3.13), Eq. (3.14) and Eq. (3.15) in Eq. (3.11), Eq. (3.11) becomes the following.

$$\begin{aligned}\frac{\partial q_{Bx}}{\partial x} &= 4\left(\tau_* - \tau_{*c}\right)^{1/2}\sqrt{sgd^3}\frac{I_e}{sd}\left[\frac{u}{V} - \frac{\gamma^{'}}{\tau_*^{1/2}}\left\{1 - \frac{1}{3\tau_*}\left(\tau_* - \tau_{*c}\right)\right\}\frac{\partial z}{\partial x}\right] \\ &\left\{\frac{\partial z}{\partial x} + I_{ex} + \frac{3}{5}\frac{u^2}{gI_{ex}}\frac{\partial I_{ex}}{\partial x} - \frac{3}{10}\frac{u^2}{gI_e}\frac{\partial I_e}{\partial x} - \frac{2}{5}\frac{uv}{gI_{ey}}\frac{\partial I_{ey}}{\partial y} - \frac{3}{10}\frac{uv}{gI_e}\frac{\partial I_e}{\partial y} + \frac{uv}{gI_{ex}}\frac{\partial I_{ex}}{\partial y} + 6\frac{h}{V}\frac{\partial V}{\partial x}\right\} \\ &+8\left(\tau_* - \tau_{*c}\right)^{3/2}\sqrt{sgd^3}\frac{1}{V}\frac{\partial u}{\partial x} - 8\left(\tau_* - \tau_{*c}\right)^{3/2}\sqrt{sgd^3}\frac{u}{V^2}\frac{\partial V}{\partial x} - 8\left(\tau_* - \tau_{*c}\right)^{3/2}\sqrt{sgd^3}\frac{\gamma^{'}}{\tau_*^{1/2}}\frac{\partial^2 z}{\partial x^2}\end{aligned} \tag{3.16}$$

In addition, $\partial q_{By}/\partial y$ is arranged in the same process as Eq. (3.16), and the following equation is obtained.

$$\begin{aligned}\frac{\partial q_{By}}{\partial y} &= 4\left(\tau_* - \tau_{*c}\right)^{1/2}\sqrt{sgd^3}\frac{I_e}{sd}\left[\frac{v}{V} - \frac{\gamma^{'}}{\tau_*^{1/2}}\left\{1 - \frac{1}{3\tau_*}\left(\tau_* - \tau_{*c}\right)\right\}\frac{\partial z}{\partial y}\right] \\ &\left\{\frac{\partial z}{\partial y} + I_{ey} + \frac{3}{5}\frac{v^2}{gI_{ey}}\frac{\partial I_{ey}}{\partial y} - \frac{3}{10}\frac{v^2}{gI_e}\frac{\partial I_e}{\partial y} - \frac{2}{5}\frac{uv}{gI_{ex}}\frac{\partial I_{ex}}{\partial x} - \frac{3}{10}\frac{uv}{gI_e}\frac{\partial I_e}{\partial x} + \frac{uv}{gI_{ey}}\frac{\partial I_{ey}}{\partial y} + 6\frac{h}{V}\frac{\partial V}{\partial y}\right\} \\ &+8\left(\tau_* - \tau_{*c}\right)^{3/2}\sqrt{sgd^3}\frac{1}{V}\frac{\partial v}{\partial y} - 8\left(\tau_* - \tau_{*c}\right)^{3/2}\sqrt{sgd^3}\frac{v}{V^2}\frac{\partial V}{\partial y} - 8\left(\tau_* - \tau_{*c}\right)^{3/2}\sqrt{sgd^3}\frac{\gamma^{'}}{\tau_*^{1/2}}\frac{\partial^2 z}{\partial y^2}\end{aligned} \tag{3.17}$$

By substituting Eq. (3.16) and Eq. (3.17) in Eq. (3.1), the following HPDE for bed level z can be derived. This equation is classified as an advection-diffusion equation because it includes a diffusion term.

$$\frac{\partial z}{\partial t} + M_x\frac{\partial z}{\partial x} + M_y\frac{\partial z}{\partial y} = D\frac{\partial^2 z}{\partial x^2} + D\frac{\partial^2 z}{\partial y^2} - M_x(I_{ex} + F_x) - M_y(I_{ey} + F_y) - F_{x2} - F_{y2} \tag{3.18}$$

In the aforementioned equation, M_x is the advection velocity of the longitudinal component of bed level z. It is assumed to be closely related to the migrating speed of the longitudinal component of the alternate bars, which is the subject of this study. M_y is the transverse migrating speed of the alternate bars. M_x and M_y are not velocities of the sediments; they are supposed to be the propagation velocities of bed level z. M_x and M_y are given as follows.

$$M_x = \frac{4(\tau_* - \tau_{*c})^{1/2}\sqrt{sgd^3}I_e}{sd(1-\lambda)}\left[\frac{u}{V} - \frac{\gamma^{'}}{\tau_*^{1/2}}\left\{1 - \frac{1}{3\tau_*}\left(\tau_* - \tau_{*c}\right)\right\}\frac{\partial z}{\partial x}\right] \tag{3.19}$$

$$M_y = \frac{4(\tau_* - \tau_{*c})^{1/2}\sqrt{sgd^3}I_e}{sd(1-\lambda)}\left[\frac{v}{V} - \frac{\gamma^{'}}{\tau_*^{1/2}}\left\{1 - \frac{1}{3\tau_*}\left(\tau_* - \tau_{*c}\right)\right\}\frac{\partial z}{\partial y}\right] \tag{3.20}$$

Eq. (3.19) and Eq. (3.20) indicate that the dominant physical quantities of the migrating speed are I_e, τ_*, and d. In addition, diffusion coefficient D, F_x, F_y, F_{x2} and F_{y2} are given as follows.

$$D = \frac{8\left(\tau_* - \tau_{*c}\right)^{3/2}\sqrt{sgd^3}}{1-\lambda}\frac{\gamma^{'}}{\tau_*^{1/2}} \tag{3.21}$$

$$F_x = \frac{3}{5}\frac{u^2}{gI_{ex}}\frac{\partial I_{ex}}{\partial x} - \frac{3}{10}\frac{u^2}{gI_e}\frac{\partial I_e}{\partial x} - \frac{2}{5}\frac{uv}{gI_{ey}}\frac{\partial I_{ey}}{\partial y} - \frac{3}{10}\frac{uv}{gI_e}\frac{\partial I_e}{\partial y} + \frac{uv}{gI_{ex}}\frac{\partial I_{ex}}{\partial y} + 6\frac{h}{V}\frac{\partial V}{\partial x} \quad (3.22)$$

$$F_y = \frac{3}{5}\frac{v^2}{gI_{ey}}\frac{\partial I_{ey}}{\partial y} - \frac{3}{10}\frac{v^2}{gI_e}\frac{\partial I_e}{\partial y} - \frac{2}{5}\frac{uv}{gI_{ex}}\frac{\partial I_{ex}}{\partial x} - \frac{3}{10}\frac{uv}{gI_e}\frac{\partial I_e}{\partial x} + \frac{uv}{gI_{ey}}\frac{\partial I_{ey}}{\partial x} + 6\frac{h}{V}\frac{\partial V}{\partial y} \quad (3.23)$$

$$F_{x2} = \frac{8\left(\tau_* - \tau_{*c}\right)^{3/2}\sqrt{sgd^3}}{1-\lambda}\left(\frac{1}{V}\frac{\partial u}{\partial x} - \frac{u}{V^2}\frac{\partial V}{\partial x}\right) \quad (3.24)$$

$$F_{y2} = \frac{8\left(\tau_* - \tau_{*c}\right)^{3/2}\sqrt{sgd^3}}{1-\lambda}\left(\frac{1}{V}\frac{\partial v}{\partial y} - \frac{v}{V^2}\frac{\partial V}{\partial y}\right) \quad (3.25)$$

3.2 Conclusion of Section 3

In this section, the HPDE for the bed level and the equation for the advection velocity are derived in order to quantify the spatial distribution of the migrating speed of alternate bars. The equations were derived by mathematical transformations of three equations: the continuity equation of bed, the bedload function and the water surface equation. The water surface equation used to derive the equation was newly derived in this study. As a result, it became possible to quantify the spatial distribution of the migrating speed of alternate bars.

4 Verifying the Applications of the HPDE for Bed Level z and the Migrating Speed Formula based on the Measured Values

In this section, we investigate the applicability of the HPDE for bed level z and its calculation formula for the migrating speed derived in the previous section.

4.1 Hydraulics Required to Verify Applicability

This section describes the hydraulic quantities required to verify the applicability of the HPDE and the calculation formula for the migrating speed, as explained in the next section. As demonstrated from the HPDE and the calculation formula for the migrating speed shown in the previous section, the hydraulic quantities required for the verification of the applicability are the water depth, energy slope, and flow velocity. The water depth can be obtained from the bed level and water level measured by the ST. However, the flow velocity and energy slope that are paired with the water depth have not been measured—this measurement is generally difficult. Therefore, we determined the flow velocity and energy slope by performing numerical analyses.

For the numerical analysis, Nays2D, included in iRIC (http://www.i-ric.org), which can solve the two-dimensional plane hydraulic analysis, was employed. The analysis was conducted with a bed level that was measured by the ST as a fixed bed. The spacing of the calculation points was 2 cm, the same as the ST resolution, in both the longitudinal and transverse directions. The upstream boundary condition was the flow rate of 1.5 L/s, and the downstream boundary condition was the measured water depth. The roughness coefficients were adjusted at each time point, such that the calculated values of the water depth and the measured values agreed with each other and were given uniformly throughout the section.

The measured values of the water depth are shown in Fig. 4.1, the difference between

the measured and calculated values of water depth is shown in Fig. 4.2, which is nondimensionalized by measurement Δh_*, and the calculated values of flow velocity are shown in Fig.4.3. Of these, Δh_* represents the computational accuracy of the numerical analysis. Considering Δh_* in Fig. 4.2, Δh_* is generally within 10% for the entire channel at all times, regardless of the development of alternate bars. All the areas where Δh_* was greater than 20% were in very shallow water.

Because Δh_* is nondimensionalized based on the measured values of water depth, it is assumed that Δh_* in this part was calculated to be large. Therefore, it is difficult to determine the computational accuracy of this part by Δh_*. However, if we focus on the calculated values of flow velocity shown in Fig. 4.3, we can obtain results that are not unnatural as a phenomenon; thus, we decided to use the calculated values of this part as well. In the next section, the applicability of the derived equations is verified using these hydraulic quantities.

4.2 Verifying the Application of the Time Waveform for the Bed Level and the Riverbed Fluctuation Amount

We verified the applicability of the calculation formula derived in the previous section from two viewpoints. First, can the time waveform of the measured bed level be reproduced? Second, can the riverbed fluctuation amount measured in the entire section be reproduced? The verification results are described in this section.

4.2.1 Bed-level Time Waveform

The verification method that uses the time waveform at the bed level is described here. Using the bed level and water depth measured by ST, and the calculated energy gradient and flow velocity from the hydraulic analysis described in the previous section, the HPDE (3.18) derived in the previous section was numerically integrated, as follows, to calculate the riverbed fluctuation between Δt.

$$\Delta z_{cal} = \left\{ -M_x \frac{\partial z}{\partial x} - M_y \frac{\partial z}{\partial y} + D\frac{\partial^2 z}{\partial x^2} + D\frac{\partial^2 z}{\partial y^2} - M_x(I_{ex} + F_x) - M_y(I_{ey} + F_y) - F_{x2} - F_{y2} \right\} \Delta t \quad (4.1)$$

A time waveform at the bed level was obtained by repeating this numerical integration during each ST measurement time.

The applicability of the HPDE obtained in the previous section was investigated by comparing the time waveform of the bed level. In this study, because the ST measurements were performed at 1-min intervals, Δt in the aforementioned calculation was set to 1 min. The method of calculating the riverbed variation amount used in the above comparison is a numerical calculation to obtain Δz after discretizing the Eq. (4.1) using the difference method.

Figure 4.4 shows the time waveform at the bed level. Figure 4.4 shows the time waveforms of (a) the left bank side, (b) central part, and (c) right bank side at 6.0 m from the upstream end. The red line shows the bed level of the measured value, and the blue line shows the bed level calculated from the formula.

Comparing the time waveform of the bed level by the calculation formula with the measured value showed that the time waveform of the bed level was well reproduced after 60 min of water flow in figures (a), (b), and (c).

As mentioned earlier, the time waveform was obtained by setting the time integration interval to 1 min. Although this time interval cannot be simply compared, it is much larger than the time interval in general numerical analysis. This result proved that the verification method that uses the aforementioned numerical integration and the applicability of the calculation formula that was derived in the previous section are excellent.

4.2.2 Riverbed Variation Amount

The verification in the previous section showed that the HPDE for Eq. (3.18) has sufficient applicability; however, its applicability decreased in the early stage of water flow. In this section, we discuss how much of this reduced applicability occupies the entire waterway and where it occurs. This is achieved using the riverbed variation amount. The

riverbed variation was verified using the following equation.

$$\Delta z_* = |\Delta z_{obs} - \Delta z_{cal}|/d \times 100 \tag{4.2}$$

where Δz_{obs} is the riverbed variation obtained from the bed level between the two times that were measured by the ST. In addition, Δz_{cal} is the amount of riverbed variation by the HPDE and the calculation formula of the migrating speed. Δz_* in the aforementioned equation is a dimensionless quantity obtained by dividing the difference between the measured value of the riverbed variation amount and the calculated value using the equation based on the particle size. In addition, the difference between the two shows how much the divergence is based on particle size.

Figure 4.5 shows a plan view for the calculation accuracy of the riverbed variation Δz_*. Figure 4.5 shows the bed level, Δz_* from the top. (a) Considering the results for 1 min of water flow, Δz_* is generally within 100%, and the estimation accuracy of the waveform after 1 min at this time is the same as the particle size. From (a) 1 min of water flow to (h) 70 min, we can see that Δz_* is generally within 100% of the entire channel. When focusing on Δz_* from (b) 10 min to (f) 50 min of water flow, areas exceeding 500% occurred periodically in the longitudinal direction, and their total area accounted for approximately 40%. The bed surface at this time showed small irregularities that correspond to the periodically increasing and decreasing Δz_*. Δz_* is within 100% in all intervals because the small irregularities disappear after (g) 60 min. The results of (a) to (g) suggest that the accuracy of the estimation of the calculation formula for the migrating speed decreases when such small irregularities exist on the bed surface. However, the mathematical reason for this is currently unknown. The subject of this study is alternate bars, and it can be said that the authors' equation has sufficient applicability in the case in which alternate bars are dominant. The authors believe that the method used in this section for the numerical calculation of the riverbed variation amount and for the validation of the substitution of measured values into the discretized equation is

appropriate. The reason for this is that if the method is essentially wrong, the riverbed variation amount estimated from the discretized HPDE and the measured values will not be consistent as shown in Figs. 8 and 9.

4.3 Conclusion of Section 4

In this section, the validity of the HPDE for the bed level and the equation for the calculating migrating speed derived in the previous section were verified by calculating the riverbed variation amount from the same equation and comparing it with the measured values. As a result, it was found that the HPDE for the bed level and the equation for calculating migrating speed derived in this study were sufficiently valid under the condition of predominant alternate bars.

5 Quantification of the Migrating Speed for the Alternate Bars

The previous section confirmed that the HPDE and calculation formula for the migrating speed can reproduce the propagation phenomenon of alternate bars. In this section, the migrating speed of the alternate bars in each process during the occurrence and development is quantified using the calculation formula of the migrating speed.

5.1 Spatial Distribution of the Migrating Speed of the Alternate Bars

Figure 5.1 shows a plan view of the dimensionless migrating speed obtained by dividing the migrating speed obtained from the calculation formula for the bed level by the initial uniform flow velocity. The dimensionless migrating speed was used to understand the magnitude of the running water velocity and bed velocity. The above is based on the fact that the governing equations are often nondimensionalized with uniform flow velocities during instability analysis [7, 11].

The figure shows the bed level and M/u_0 from the top. M is the magnitude migrating speed, and u_0 is the uniform flow velocity. The area surrounded by the hatch in the figure is the area in which the Shields number does not exceed the critical Shields number (hereinafter referred to as the effective Shields number); in this area, the migrating speed is 0.

First, by focusing on (a) 1 min of water flow in the figure, M/u_0 has almost no spatial distribution on a floor with an almost flat bed. We also confirmed that the bed surface uniformly propagates at a speed of approximately 0.0015. After the bed changes slightly from (b) 10 min to (e) 40 min, M/u_0 begins to show spatial distribution. Subsequently, the spatial distribution of M/u_0 changes significantly from (g) 60 min of water flow to (l) 110 min. Considering this change with a spatial distribution from place to place, it can

be seen that M/u_0 increases at the sedimentary part and the front edge of the alternate bars, and it decreases at other locations.

Next, Fig. 5.2 illustrates a histogram that quantitatively shows the spatial distribution degree of M/u_0 at each time. The red and blue vertical lines in the figure represent the mean $\pm$ and standard deviation of M/u_0 at each time, and each value is shown at the top of the figure. First, (a) the shape of the histogram after 1 min of water flow is concentrated around an average value of 0.00143. In addition, because the standard deviation is 0.00015, which is small with respect to the mean value, it can be observed that the spatial distribution of M/u_0 at this time was small. Then, from (b) 10 min of water flow to (g) 60 min of water flow when the alternate bars occurred, the shape of the histogram became flat; the mean value of M/u_0 was 0.00126, and the standard deviation was 0.00023. Comparing (a) 1 min and (g) 60 min of water flow showed that although the mean value decreased by approximately 12 %, the standard deviation increased to nearly 1.5 times. This shows that the spatial distribution of the migrating speed greatly expanded from the flat bed to the occurrence of the alternate bars. After that, from (g) 60 min to (l) 110 min of water flow, the flattening of the histogram, the increase in the standard deviation, and the decrease in the mean value of M/u_0 became more significant. Comparing (a) 1 min of water flow and (l) 110 min, which was the final time, showed that the mean value of M/u_0 of (l) is 0.78 times from (a), and the standard deviation of (l) is 2.4 times from (a).

These results demonstrated that the migrating speed of the alternate bars has a spatial distribution, which expands from the stage of occurrence to the development of the alternate bars.

5.2 Scale of the Migrating Speed of the Alternate Bars

This section discusses the scale of the migrating speed of the alternate bars. As shown in the previous section, from Fig. 5.2, it can be confirmed that the migrating speed has

a spatial distribution, which gradually expands from 1 min of water flow to 110 min. The non-dimensional migrating speed in the figure is divided by the uniform flow velocity on the flat floor. The scale of the migrating speed is in the order of 10^{-4} to 10^{-3} of the uniform flow velocity at any location, regardless of the developmental state of the alternate bars. Therefore, it is inferred that the deformation rate of the bed surface is sufficiently smaller than the deformation rate of running water.

5.3 Main Dominant Physical Quantity of Migrating Speed and Approximate Description of Migrating Speed

5.3.1 Main Dominant Physical Quantity

In this study, the migrating speed of alternate bars is quantified by both measurements and estimations. The validity of the calculated migrating speed is also confirmed. In this section, we discuss the mathematical structure of the equation to understand the main dominant physical quantity of the migrating speed.

Fig. 5.3 shows three relationships between the energy slope, the Shields number, and the dimensionless migrating speed at the final time of the flume experiment. The same figure indicates that the dimensionless migrating speed is proportional to the Shields number and energy slope. Because the dimensionless migrating speed is a product of Shields number and energy slope, it is difficult to say which is dominant. However, in this experiment, the energy slope is closer to the order of the dimensionless migrating speed, indicating that the energy slope is the more dominant physical quantity.

5.4 Approximate Description

In the previous section, we suggested that the energy slope is the dominant physical quantity that determines the order of migrating speed. From this, it can be inferred that the energy slope can be used to describe the approximate migrating speed. Whether

this approximate description is possible was examined based on the relationship between M/u_0 and $0.4 \times I_e$ in Fig. 5.4. The correlation coefficients between the two at each time are shown in the figure. The value of 0.4 multiplied by the same equation is a coefficient determined from the particle size, which is one of the variables in the denominator of equations (3.19) and (3.20).

Considering the relationship between M/u_0 and $0.4 \times I_e$, we can see that the relationship is almost one-to-one at all times. The correlation coefficients are above 0.9 on average, indicating that the two have a strong positive correlation. These results suggest that an approximate description of the migrating speed of alternate bars using energy slope is possible.

5.5 Decreasing Factor for the Migrating Speed of the Alternate Bars

This subsection discusses the decreasing factor for migrating speed of the alternate bars. Figure 5.5 shows the average longitudinal distributions of the (a) migrating speed, (b) energy line, hydraulic grade line, and bed line over time. The sediment condition for the flume experiment in this study is that no sediment supply exists. Therefore, the bed level and each hydraulic head decreased with time in the upstream section of the moving bed. The water level and energy head in the same section also decreased from the initial stage, and the water surface slope and energy slope, including the riverbed slope, became more moderate. In contrast, the water depth did not change much from the initial value in the whole section. In addition, it can be seen that (a) the migrating speed in the same section decreased from the initial value. Next, if we focus on the point 5.5 m from the upstream end, we can see that the water depth has hardly changed since the initial value, the energy slope has increased, and the migrating speed has also increased.

As shown in Eq. (3.19) and Eq. (3.20), there are three dominant physical quantities of the migrating speed, which are grain size, non-dimensional scavenging force, and energy

gradient, except for the component decomposition part. The dominant physical quantities of the Shields number are grain size, water depth, and energy slope. Therefore, we can say that there are three physical quantities that effectively govern the migrating speed, which are grain size, water depth, and energy slope. Focusing on these dominant physical quantities, the decreasing factors of the migrating speed of alternate bars in this experiment can be summarized as follows. First, because the particle size in this experiment is a single particle size, it is assumed that there is no change in the migrating speed due to changes in the particle size. Because the water depth also slightly changed on average, it can be inferred that there was little change in the migrating speed due to changes in the water depth. In contrast, the energy slope was significantly reduced, and the migrating speed was considerably decreased along with it. This decrease in the energy slope is due to the decrease in the bed level caused by the no sediment supply at the upstream end. These results indicate that the reason for the decrease in the migrating speed of the alternate bars in this experiment is the decrease in the energy slope due to the decrease in the bed slope.

Eekhout et al. [29] observed the occurrence and development processes of alternate bars in an actual river and reported that the bed slope decreased when the migrating speed of alternate bars was decreased. The migrating speed of the alternate bars decreased owing to changes in grain size or water depth because their study had the same target section and the same flood magnitude during the observation period. Based on the results of this experiment, we assumed that the migrating speed decreased owing to the reduction in the energy slope caused by a decrease in the bed slope.

5.6 Comparison of the Migrating Speed of our Method with that of Instability Analysis

The conditions for the occurrence and non-occurrence of alternate bars have been determined by instability analysis for small perturbations given as initial conditions [7, 11].

In these instability analyses, the migrating speed of small perturbations was calculated. Although the form of the equation and the process of deriving the equation are different, it can be inferred that the equation for migrating speed based on instability analysis and the equation for migrating speed in this study were essentially the same. In this section, we compare the migrating speed of our method with that of instability analysis.

Fig. 5.6 shows the relationship between the migrating speed of our method and the migrating speed of instability analysis. The vertical axis of the figure is the migrating speed of our method, which is shown as a box-and-whisker diagram for three time periods: 1 min at the initial river bed, 50 min at the time of sandbar occurrence, and 120 min at the final time under each hydraulic condition shown in Table 2.1. The horizontal axis of the figure is the migrating speed for the instability analysis and shows the results of each of the linear and weakly nonlinear analyses obtained when the same hydraulic conditions were given as in Table 2.1. The migrating speed for instability analysis was calculated from the equation proposed by Bertagni [17], shown below.

$$M_{*(\mathrm{L.})} = -\frac{\mathrm{Im}[\Omega]}{k} \tag{5.1}$$

$$M_{*(\mathrm{W.N.L.})} = -\left(\frac{\mathrm{Im}[\Omega] - \mathrm{Im}[\Xi]\frac{\mathrm{Im}[\Omega]}{\mathrm{Re}[\Xi]}}{k}\right) \tag{5.2}$$

where $M_{*(\mathrm{L.})}$ is the non-dimensional migrating speed from linear instability analysis, $M_{*(\mathrm{W.N.L.})}$ is the non-dimensional migrating speed from weakly nonlinear instability analysis, Ω is the amplification factor, k is the wavenumber, and Ξ is the Landau Coefficient. For details on how to calculate the amplification factor Ω and Landau Coefficient Ξ, please refer to the original publication [17].

(a) to (c) in the same figure show the migrating speed of each bars from the occurrence to the development stage. First, the vertical axis of (a) to (c) in the same figure shows that the migration speed of the authors decreased on average from the occurrence to the

development of the alternate bars. Next, focusing on the migration speed of the instability analysis, the migrating speed of the weakly nonlinear instability analysis is slower than that of the linear instability analysis. The migrating speed of the linear instability analysis is those of the dominant wave number at the time of alternate bars occurrence, while the migrating speed of the weakly nonlinear instability analysis is those of the dominant wave number at the time of alternate bars development. Thus, the trend of the migrating speed of the alternate bars from the occurrence to the development is consistent between the author's method and the instability analysis.

In the previous section and in Fig. 5.2, we have shown that the migrating speed of alternate bars has a spatial distribution and that it varies with time. Nevertheless, the migrating speeds is generally the same regardless of the time of occurrence and the stage of development. The reason for this is that, as can be seen immediately from Fig. 5.2, the scale of the change in the spatial distribution of the migrating speed during the development stage of the alternate bars is not much different from that during the occurrence of the alternate bars, and the statistical variance is as small as 10^{-3}.

5.7 Conclusion of Section 5

In this section, we quantified the migrating speed of alternate bars during their occurrence and development by using the derived calculation formula for migrating speed. As a result, it was clarified that the migrating speed of alternate bars has spatial distribution and expands from the occurrence to the development of alternate bars. As a result of comparing the migrating speed with the uniform flow velocity, it was found that the migrating speed was in the order of 10^{-4} to 10^{-3} of the uniform flow velocity regardless of the state of the alternate bars, and the deformation velocity of the bed was sufficiently small compared with the deformation velocity of the flowing water.

Furthermore, the mathematical structure of the equation revealed that the energy slope is the main dominant physical quantity of the migrating speed, and that the decrease of

the migrating speed is caused by the decrease of the energy slope with the decrease of the bed slope.

Finally, a comparison between the migrating speed of the instability analysis and that of the our method shows that the trend of the migrating speed from the occurrence to the development of the alternate bars is consistent between the our method and the instability analysis.

6 Applicability of the Formula for Calculating Migrating Speed in Actual Rivers

The validity of the formula of migrating speed derived in the previous section was confirmed by measurements in flume experiments, and the spatial distribution of the migrating speed was quantified. In this section, we investigate the applicability of the formula to an actual river, where the scale, bed material, and hydraulic conditions are completely different from those in the flume experiment.

6.1 Migrating phenomena of alternate bars in Chikuma River during Typhoon 19 in 2019.

6.2 Flood Summary for Target River

The study river was the Chikuma River, which flows through Nagano Prefecture, Japan, as shown in Fig. 6.1(a). It is the longest river in Japan, with a channel length of 300 km. Owing to the outflow of water caused by Typhoon No. 19 in October 2019, the water level remained close to the bank level for approximately 10 h (Fig. 6.2(b)). This is the largest flow ever recorded and the eighth highest water level ever recorded in the history of observation.

Figure 1.1(a),(b) are aerial photographs of the river channel before and after the outflow in Ueda City shown in Fig. 6.1(b). The same figure shows that the alternate bars in the river channel were moved on a large scale by the outflow of water. The light blue line and the blue line in (b) of the same figure show the water route before and after the flood, respectively. Because the position of the water route depends on the position of the alternate bars, the distance moved by the water route at the time of outflow can be considered as the distance moved by the alternate bars before and after the flood, and it can be confirmed that the alternate bars traveled 450 to 800 m during this outflow.

6.2.1 Reproduction Calculations for Typhoon 19 in 2019

6.2.2 Governing Equation

To calculate the migrating speed obtained using our formula, one-dimensional unsteady flow calculations for a general cross section were performed to calculate the hydraulic quantities required for the calculations. The governing equations used in this calculation are the following two. The reason for the one-dimensional analysis is that it is difficult to obtain detailed information necessary for hydraulic calculations for actual rivers.

$$\frac{\partial A}{\partial t} + \frac{\partial Q}{\partial x} = 0 \tag{6.1}$$

$$\frac{\partial Q}{\partial t} + \frac{\partial}{\partial x}\left(\frac{Q^2}{A}\right) + gA\frac{\partial}{\partial x}(z+h) + \frac{gn^2u^2S}{R^{1/3}} = 0 \tag{6.2}$$

where A is the flow area, Q is the flow discharge, t is the time, x is the distance, z is the bed level, h is the water depth, n is Manning's roughness coefficient, and R is the hydraulic mean depth.

6.3 Calculation Conditions

The target interval was from the 84-km point at Kuiseshita Observatory to the 109.5-km point at Ikuta Observatory, as shown in Fig. 6.1(b). For this calculation, we used transect survey data obtained at 500-m intervals and measured in 2017. Notably, from 2017, when the survey was conducted, to 2019, when the water was released, the river had not experienced any water outflow that would have significantly altered the channel geometry. The river bed material was given by varying it as a linear function in the computational section because it was 20 mm at the downstream end and 70 mm at the upstream end of the computational section. The roughness coefficient was given by the Manning–Strickler equation. The upstream boundary condition is the flow discharge at

Ikuta Observatory, shown in Fig. 6.2(a), and the downstream boundary condition is the water level at Kuisenshita Observatory, shown in Fig. 6.2(b).

6.3.1 Calculation Formula for Migrating Speed

Using the hydraulic quantities obtained from the above calculations, the migrating speed was calculated using the following equation. The same equation is a uni-dimensionalized expression obtained by finding the composite component of equations (3.19) and (3.20).

$$M = \frac{4(\tau_* - \tau_{*c})^{1/2}\sqrt{sgd^3}I_e}{sd(1-\lambda)}\left[1 - \frac{\gamma^{'}}{\tau_*^{1/2}}\left\{1 - \frac{1}{3\tau_*}(\tau_* - \tau_{*c})\right\}\frac{\partial z}{\partial x}\right] \tag{6.3}$$

6.3.2 Calculation Result

Fig. 6.3 shows the longitudinal distribution of the estimated and measured migrating speed, and the same figure shows the interval of the calculation in Fig. 1.1. The green line in the figure shows the calculation results at each flow discharge marked in Fig. 6.2, from 1000 m^3/s, when sediment began moving throughout the section, to the peak flow discharge. The migrating speed was calculated using the uni-dimensionalized migrating speed equation shown in equation (6.3), using the hydraulic mean depth, energy slope, and Shields number. The gray marks in the figure indicate the measured migrating speed. The average migrating speed during the flood period was calculated based on the relationship between the travel distance of the water route and the travel time, which was assumed to be approximately 29 h of active sediment transport based on the flow hydrograph and analysis results.

Focusing on the calculation results of the migrating speed at each flow discharge, we can see that the migrating speed has a spatial distribution at all flow discharge, and it increases as the flow discharge increases.

A comparison of the calculated and measured migrating speeds confirms that the calculated values are about half of the measured values, but they are generally consistent with

the measured values, and the waveforms are also generally consistent, except for those at the 104-km point. These results suggest that the hydraulic quantity in the downstream direction is dominant in defining the migrating speed.

6.4 Conclusion of Section 6

In this section, the theoretical equation for the migrating speed of an alternate bars was applied to an actual river and compared with the migrating speed of bars that actually migrated in the actual river. As a result, it was confirmed that the calculated values based on the theoretical equation agreed well with the actual measured values.

7 Conclusion

7.1 Results obtained in This Study

In Section 1, the background and purpose of this study are first presented, and it is summarized that the migration of alternate bars is poorly understood, especially the spatial distribution of the migrating speed and the their dominant physical quantities are unknown. Next, the hydrological phenomena covered in this study are described, and the academic and engineering importance of this study is discussed.

In Section 2, flume experiments were conducted under the hydraulic conditions where alternate bars develop and migrate, and the existence of spatial distribution of the migrating speed of alternate bars was investigated based on the measurements. Based on the measurement results, it was confirmed that the alternate bars migrated with changing its shape. The results were discussed based on the wave theory, and it was found that the alternate bars have a nonlinear wave property in that its migrating speed is spatially distributed and changes with time. This indicates that the migrating speed of the alternate bars have a spatial distribution.

In Section 3, the hyperbolic partial differential equation (HPDE) for the bed level of the alternate bars is derived, assuming that the alternate bars can be regarded as a wave phenomenon, in order to quantify the spatial distribution of the migrating speed of them. By formulating the advection velocity given to the advection term in the same equation, an equation for calculating the migrating speed of the alternate bars was derived.

In Section 4, the validity of HPDE for the bed level z derived in Section 3 and the equation for calculating the migrating speed are examined from two points of view based on ST measurements and numerical analysis: 1) whether the equation can reproduce the measured time waveform of the bed level, and 2) whether the equation can reproduce the measured riverbed variation amount in the entire section.

From the above verification results, it is shown that the authors' equation has sufficient applicability in the case of predominantly alternate bars, although the estimation accuracy

of the equation for calculating the migrating speed decreases when small irregularities exist on the bed.

In Section 5, we quantified the migrating speed of alternate bars during their occurrence and development using the derived calculation formula for migrating speed. As a result, it was found that the migrating speed of alternate bars has a spatial distribution, and this spatial distribution expands during the development of alternate bars.

Next, the results of comparing the migrating speed with the uniform flow velocity showed that the migrating speed was on the order of 10^{-4} to 10^{-3} of the uniform flow velocity regardless of the condition of the alternate bars, and the deformation velocity of the bed was sufficiently small compared to the deformation velocity of the flowing water.

In addition, the mathematical structure of the equation revealed that the energy slope is the main dominant physical quantity of the migrating speed, and that the decrease of the migrating speed is caused by the decrease of the energy slope with the decrease of the bed slope.

Finally, a comparison between the migrating speed of the instability analysis and that of the present method suggests that they have the same magnitude and are essentially the same. The migrating speed of the alternate bars has a spatial distribution, which changes with time. Nevertheless, regardless of the time of occurrence and the stage of development of the bars, the migrating speed of both is generally consistent. The reason for this is that the scale of the change in the spatial distribution of the migrating speed at the stage of development of the alternate bars is not much different from that at the time of the occurrence of the alternate bars, and the statistical variance is as small as 10^{-3}.

In Section 6, the theoretical equation for the migrating speed of an alternate bars is applied to an actual river and compared with the migrating speed of the bars that actually migrated in the actual river. As a result, it was confirmed that the calculated values based on the theoretical equation agreed well with the measured values. This method is expected to enable the understanding and prediction of the migration of alternate bars, which is necessary for countermeasures against erosion and scouring type embankment damage.

7.2 Academic Significance of Results in This Study

7.2.1 Demonstration of the Validity of Pseudo-Fixed Beds

As mentioned in 1.3.1, to demonstrate the validity of the pseudo-fixed bed, it is necessary to quantify the spatial distribution of the migrating speed of the bed and to prove that the deformation speed (migrating speed) of the bed is sufficiently slow compared to the deformation speed (flow velocity) of the flowing water. However, there has been no method to quantify the spatial distribution of the migrating speed of the bed.

As mentioned in the second conclusion of Section 5 in the previous subsection, the results of comparison between the migrating speed and the uniform flow velocity showed that the migrating speed was on the order of 10^{-4} to 10^{-3} of the uniform flow velocity regardless of the state of the alternate bars, and the deformation speed of the bed was sufficiently slow compared to the deformation speed of the flowing water. This indicates that the assumption of a pseudo-fixed bed is valid for the alternate bars in this study.

7.2.2 Demonstration of the Validity of Previous Mathematical Analyses

As described in Section 1.3.2, the migrating speed obtained from instability analysis are calculated for each wave number. For this reason, the this migrating speed cannot be used to calculate the migrating speed of a synthetic wave with various wave numbers, such as an alternate bars. For this reason, it has been unclear what kind of migrating speed obtained from instability analysis corresponds to the migrating speed of alternate bars during its occurrence and development. In this study, alternate bars are regarded as a kind of wave phenomenon, and a hyperbolic partial differential equation is newly derived to describe the wave phenomenon there. The advection velocity assigned to the advection term in the equation can be used to directly describe the migrating speed of the alternate bars. By this change of idea, we succeeded in directly estimating the migrating speed of the alternate bars, which is a composite wave of various wave numbers, from the velocity of each wave number by instability analysis.

The last of the conclusions of Section 5 in the previous subsection provides one answer to the questions in this subsubsection. Since the migrating speed obtained by author's method and those by the instability analysis generally agree, we can say that the migrating speeds obtained from the instability analysis are average or representative of the migrating speed of alternate bars.

In addition, the validity of the quasi-steady flow assumption applied in the instability analysis can now be shown. In addition, we have been able to demonstrate the sufficient validity of researches, which is that proposes a unified classification of three riverbed waves based on wave theory assuming a fixed bed[36] and, which estimated the geometric shape of the bed from the minute amplitude of the water surface by data-driven analysis[37].

7.3 Engineering Significance of Results in This Study

In this study, the applicability of the author's equation for calculating migrating speed was verified in flume experiments, and the applicability of the equation was also verified in an actual river with completely different scale, riverbed materials, and hydraulic conditions from flume experiments. As a result, the applicability of the equation was confirmed in actual rivers.

In this study, we confirmed the applicability of the one-dimensional equation of the migrating speed using the hydraulic quantities obtained from one-dimensional hydraulic calculations. By applying this method in the spring before the runoff season, it is possible to estimate which section of bars will be migrated by a flood of what magnitude. In other words, the results of this study enable us to determine for the first time whether or not and how large alternate bars will migrate, which is an important factor in taking countermeasures against erosion and scour type damage.

8 Reference Article

Journal of JSCE, Ser. A2 (Applied Mechanics (AM)) (peer-reviewed)

1. Michihide, Ishihara and Hiroyasu Yasuda:ON THE SPATIAL DISTRIBUTION OF ALTERNATE BARS'S CELERITY AND ITS TEMPORAL VARIATION, Journal of JSCE, Ser. A2 (Applied Mechanics (AM)), Vol.76, No.2, I_469-I_480, 2020.

Journal of JSCE, Ser. B1 (Hydraulic Engineering) (peer-reviewed)

1. Michihide, Ishihara and Hiroyasu, Yasuda and Takumi, Igarashi:ON THE DECREASING FACTOR OF ALTERNATE BARS CELERITY, Journal of JSCE, Ser. B1 (Hydraulic Engineering)(in Japanese), Vol.74, No.4, pp.I_1111–I_1116, 2018.

Advances in River Engineering (peer-reviewed)

1. Kaori, Ishizuka and Michihide, Ishihara and Hiroyasu, Yasuda:DEVELOPMENT OF A MULTI-LAYERED ESTIMATION METHOD FOR DANGEROUS SECTION IN SAND BAR RIVERS, Advances in River Engineering (in Japanese), Vol.27, pp.523–528, 2021.

2. Michihide Ishihara and Hiroyasu Yasuda and Suguru Saito:ESTIMATION OF FORESTATION AVOIDANCE TOPOGRAPHY ON DYNAMIC EQUILIBRIUM STATE OF BED, Advances in River Engineering (in Japanese), Vol.25, pp.617-622, 2019.

9 Related Article

Advances in River Engineering（peer-reviewed）

1. Yakumi, Igarashi and Michihide, Ishihara and Hiroyasu Yasuda and Yasutaka, Motomura and Kazuki Takeishi:HYDRODYNAMICS ESTIMATION OF WEAK SECTION IN RIVER CHANNEL FOR MAINTENANCE AND INSPECTION, Advances in River Engineering (in Japanese), Vol.25, pp.617-622, 2019.

土木学会関東支部新潟会研究調査発表会論文集（査読なし）Only Japanese Title

1. 石原道秀，安田浩保：交互砂州上の流れを再現する数値計算に要求される空間分解能, 第 39 回土木学会関東支部新潟会研究調査発表会論文集, 2021.
2. 石原道秀，安田浩保：移動床における擬似固定床の物理的考察, 第 38 回土木学会関東支部新潟会研究調査発表会論文集, 2020.
3. 石原道秀，安田浩保：流路変動の発生過程における交互砂州の伝播に関する考察, 第 38 回土木学会関東支部新潟会研究調査発表会論文集, 2020.
4. 石原道秀，安田浩保：河床波の伝播速度の時空間分布の理論的な評価, 第 37 回土木学会関東支部新潟会研究調査発表会論文集, 2019.
5. 黛由季，石原道秀，安田浩保：実測値に基づいた掃流砂量と無次元掃流力の対応関係に関する考察, 第 37 回土木学会関東支部新潟会研究調査発表会論文集, 2019.
6. 茂木大知，安田浩保，石原道秀，早坂圭司：Optical-Flow を用いた表面流速測定手法の開発と砂水路床における適用性の検証 第 37 回土木学会関東支部新潟会研究調査発表会論文集, 2019.
7. 石塚芳，安田浩保，石原道秀：側岸の侵食性の有無が流況や底面形状に与える影響の把握, 第 37 回土木学会関東支部新潟会研究調査発表会論文集, 2019.
8. 梅木康太朗，安田浩保，石原道秀：拡縮工法の効果範囲の水理学的な推定法について, 第 37 回土木学会関東支部新潟会研究調査発表会論文集, 2019.

9. 佐々木靖幸，安田浩保，石原道秀：氾濫計算における移流項の重要性について, 第37回土木学会関東支部新潟会研究調査発表会論文集, 2019.

10. 石原道秀，安田浩保：交互砂州の流下状態の理論的な評価について, 第36回土木学会関東支部新潟会研究調査発表会論文集, pp.100-pp.103, 2018.

11. 安田浩保，石原道秀：能生川における河道内の脆弱点の推定, 第36回土木学会関東支部新潟会研究調査発表会論文集, pp.108-pp.109, 2018.

12. 石原道秀，安田浩保，五十嵐拓実：十分に発達した交互砂州の移動停止条件の解明, 第35回土木学会関東支部新潟会研究調査発表会論文集, pp.90-pp.93, 2017.

10 Acknowledgments

Dr. Hiroyasu Yasuda, Associate Professor at the Research Institute for Natural Hazards and Disaster Recovery, Niigata University, gave me guidance on my research for five years from the first year of my master's degree, and also provided me with a wide range of guidance on the basic mental attitude that I should have as a human being. He also helped me to make up my mind about my future career as a researcher and to think about my future life together. I would like to express my deepest gratitude to him.

I would like to express my deepest gratitude to the members of the River Engineering Laboratory of Niigata University for their invaluable assistance in model experiments and numerical analyses during the course of this research.

I would like to express my deepest gratitude to Dr. Shoji Okada, Associate Professor at Associate Professor, Department of Social Design Engineering, National Institute of Technology, Kochi College, for providing me with such a wonderful laboratory to go to when I was worried about my future. I would like to express my deepest gratitude to him.

Finally, I would like to express my gratitude to my parents and all other family who have supported me throughout my 12 years as a student, including my time at the National College of Technology.

11 References

[1] Seminara, G.:Fluvial Sedimentary Patterns, *Annual Review of Fluid Mechanics*, Vol.42, No.1, pp.43–66, 2010.

[2] Kinoshita, Ryosaku:Investigation of channel deformation in Ishikari river, Rep. Bureau of Resources, Dept. Science & Technology, Japan. (in japanese), 1961.

[3] Fujita, Y. and Muramoto, Y.:Experimental Study on Stream Channel Processes in Alluvial Rivers, Bulletin of the Disaster Prevention Research Institute, Vol.32, No.1, 1982.

[4] Ikeda, H.:Experiments on bedload transport,bed forms,and sedimentary structures using fine gravel in the 4-meter-wide flume, 1983.

[5] Fujita, Y. and Muramoto, Y:Studies on the Process of Development of Alternate Bars, *Bulletin of the Disaster Prevention Research Institute*, Vol.30(3), pp.55–86, 1985.

[6] Nagata, Nobuhisa and Muramoto, Yoshio and Uchikura, Yoshihiko and Hosoda, Takashi and Yabe, Masayuki and Takada, Yasuhiko and Iwata, Michiaki:ON THE BEHAVIOUR OF ALTERNATE BARS UNDER SEVERAL KINDS OF CHANNEL CONDITIONS, PROCEEDINGS OF HYDRAULIC ENGINEERING (in japanese), Vol.43, pp.743–748, 1999.

[7] Callander, R. A.:Instability and river channels, *J. Fluid Mech.*, No.3, pp.465–480, 1969.

[8] Kennedy, John F.:The mechanics of dunes and antidunes in erodible-bed channels, *J. Fluid Mech.*, Vol.16, No.4, pp.521–544, 1963.

[9] Hayashi, Taizou and Ozaki, Yukio and Onishi, Koyo:On the Mechanism of Occurrence of Three-Dimensional Bed Configurations, PROCEEDINGS OF THE JAPANESE CONFERENCE ON HYDRAULICS (in japanese), Vol.26, pp.17–24, 1982.

[10] Ozaki, Sachio and Hayashi, Taizo:On the Formation of Alternating Bars and Braids and the Dominant Meander Length, Proceedings of the Japan Society of Civil Engineers, No.333, pp.109–118, 1983.

[11] Kuroki, Mikio and Kishi, Tsutomu:Regime Criteria on Bars and Braids in Alluvial Straight Channels, Proceedings of the Japan Society of Civil Engineers (in Japanese), No.342, pp.87–96, 1984.

[12] Colombini M., Seminara G, Tubino M.:Finite-amplitude alternate bars, *J. Fluid Mech.*, 181:213–232, 1987.

[13] Colombini M., Tubino, M.:Finite-amplitude free bars: A fully nonlinear spectral solution, *in Sand Transport in Rivers, Estuaries and the Sea, edited by R. Soulsby and R. Bettes*, A. A. Balkema, Brookfield, Vt., pp.163–169, 1991.

[14] Tubino, M:Growth of alternate bars in unsteady flow, *Water Resource Research*, Vol.27, No.1, pp.37–52, 1991.

[15] R. Schielen and A. Doelman and H. E. Swart:On the nonlinear dynamics of free bars in straight channels, *J. Fluid Mech.*, Vol.252, pp.325–356, 1993.

[16] Izumi, Norihiro and Pornprommin, Adichai:Weakly Nonlinear Analysis of Bars with the Use of The Amplitude Expansion Method, Journal of JSCE (in Japanese), No.712, pp.73–86, 2002.

[17] Bertagni, Matteo Bernard and Camporeale, Carlo:Finite Amplitude of Free Alternate Bars With Suspended Load, Water *Resources Research*, Vol.54, No.12, pp.9759–9773, 2018.

[18] Shimizu, Y. and Itakura, T.:Calculation of Bed Variation in Alluvial Channels, *J. Hydraulic Eng.*, Vol.115, No.3, pp.367–384, 1989.

[19] Federici B, Seminara G.:On the convective nature of bar instability. *J. Fluid Mech.* 487:125–45, 2003.

[20] Lanzoni, Stefano:Experiments on bar formation in a straight flume: 1. Uniform sediment, *Water Resource Res.*, Vol.36, No.11, pp.3337–3349, 2000.

[21] Lanzoni, Stefano:Experiments on bar formation in a straight flume: 2. Graided sediment, *Water Resource Res.*, Vol.36, No.11, pp.3351–3363, 2000.

[22] Miwa, Hiroshi and Daido, Atsuyuki and Katayama, Tomohito:Effects of Water and Sediment Discharge Conditions on Variation in Alternate Bar Morphoroly, Proceedings of hydraulic engineering (in japanese), Vol.51, pp.1051–1056, 2007.

[23] Crosato, A., E. Mosselman, F. Beidmariam Desta, and W. S. J. Uijttewaal:Experimental and numerical evidence for intrinsic nonmigrating bars in alluvial channels, *Water Resour. Res.*, Vol.47, No.3, 2011.

[24] Crosato, Alessandra and Desta, Frehiwot Beidmariam and Cornelisse, John and Schuurman, Filip and Uijttewaal, Wim S. J.:Experimental and numerical findings on the long-term evolution of migrating alternate bars in alluvial channels, *Water Resource Res.*, Vol.47, No.6, 2012.

[25] Venditti, J. G., P. A. Nelson, J. T. Minear, J. Wooster, and W. E. Dietrich:Alternate bar response to sediment supply termination, *J. Geophys. Res.*, 117, F02039, doi:10.1029/2011JF002254, 2012.

[26] Podolak C. J. P. and Wilcock P. R.:Experimental study of the response of a gravel streambed to increased sediment supply, *Earth Surf. Process. Landforms*, 38, 1748–1764, 2013.

[27] Bankert, Andrew R. and Nelson, Peter A.:Alternate bar dynamics in response to increases and decreases of sediment supply, *Sedimentology*, Vol.65, No.3, pp.702–720, 2018.

[28] Nelson, Peter and Morgan, Jacob:Flume experiments on flow and sediment supply controls on gravel bedform dynamics, *Geomorphology*, Vol.323, 2018.

[29] J.P.C. Eekhout et al. Field experiment on alternate bar develpoment in a straight sand-bed stream, *Water Resour. Res.*, Vol. 49, 8357–8369, doi:10.1002/2013WR014259, 2013.

[30] Adami, Luca and Bertoldi, Walter and Zolezzi, Guido:Multidecadal dynamics of alternate bars in the Alpine Rhine River, *Water Resour. Res.*, Vol. 52, No.11, pp.8938–8955, 2016.

[31] Iwagaki, Yuichi:Hydrodynamical study on critical tractive force, Transactions of the Japan Society of Civil Engineers (in Japanese), No.41, pp.1–21, 1956.

[32] Dataset, https://doi.org/10.4121/16788778.v1.

[33] Hoshino, Tsuyoshi and Yasuda, Hiroshi and Kurahashi, Masayuki:Direct measurement method of formation processes of alternate bars, J. Jpn. Soc. Civ. Eng. Ser. Applied Mechanic A2.(in Japanese), Vol.74, No.1, pp.63–74, 2018.

[34] Michihide, Ishihara and Hiroyasu, Yasuda and Takumi, Igarashi:ON THE DECREASING FACTOR OF ALTERNATE BARS CELERITY, Journal of Japan Society of Civil Engineers, Ser. B1 (Hydraulic Engineering)(in Japanese), Vol.74, No.4, pp.I_1111–I_1116, 2018.

[35] Dey, Subhasish and Ali, Sk Zeeshan:Fluvial instabilities, Physics of Fluids, Vol.32, No.6, pp.061301, 2020.

[36] Hiroshi KOSEKI and Hiroyasu YASUDA:UNIFIED DIAGRAM ON SAND WAVES USING DEPTH–WAVELENGTH RATIO, Journal of Japan Society of Civil Engi-

neers, Ser. A2 (Applied Mechanics (AM))(in Japanese), Vol.76, No.2, pp.I_489–I_498, 2020.

[37] Kaneko Y, Muramatsu S, Yasuda H, Hayasaka K, Otake Y, Ono S, Yukawa M:Convolutional-Sparse-Coded Dynamic Mode Decomposition and Its Application to River State Estimation, Proc. of 2019 IEEE International Conference on Acoustics, Speech and Signal Processing (ICASSP), pp.1872-1876, 2019.

[38] 千曲川堤防調査委員会:千曲川堤防調査委員会報告書, (https://www.hrr.mlit.go.jp/river/chikumagawateibouchousa/chikuma-houkokusyo-isshiki.pdf), 2020.

[39] 国土技術研究センター:河川計画検討の手引き, (https://www.jice.or.jp/cms/kokudo/pdf/tech/material/kadoukeikaku.pdf), 2002.

[40] Watanabe, Akihide and Fukuoka, Shoji and Yasutake, Yu and Kawaguhi, Hiroshi:GROIN ARRANGEMENTS MADE OF NATURAL WILLOWS FOR REDUCEING BED DEFORMATION IN A CURVED CHANNEL, Advances in river engineering (in japanese), Vol.7, pp.285–290, 2001.

[41] River Center of Hokkaido, http://i-ric.org.

12 Appendix

12.1 Appendix A：Validity of the Pseudo-steady Flow Assumption Applied to Bars-Scale Riverbed Waves

This section describes the validity of the pseudo-steady flow assumption applied to the bar-scale riverbed waves. In this study, we introduced the assumption of a pseudo-steady flow when deriving the HPDE for bed level z. This assumption is often introduced in stability analyses of bar-scale riverbed waves [7, 11]. In the aforementioned stability analysis, we assumed that the migrating speed of the bed is sufficiently slower than the propagation velocity of the flow, and the flow can be treated as a pseudo-steady flow if the flow rate is constant. Based on this assumption, for stability analysis, we ignore the term of the time gradient in the continuity equation of flow and the equation of motion of flow among the governing equations that are used in the analysis. The aforementioned assumptions are considered to be valid. This is because the stability analysis explains the occurrence and developmental mechanisms of alternate bars. However, to the best of our knowledge, whether the term of the time gradient of the flow can actually be ignored cannot be confirmed from the actual phenomenon. Therefore, we verified whether the term of the flow time gradient can be ignored with ST measurement values and hydraulic analysis.

12.1.1 Verification Method

The aforementioned verification was performed by comparing the contributions of each term in the equation of motion for flow.

$$\frac{1}{g}\frac{\partial u}{\partial t} + \frac{u}{g}\frac{\partial u}{\partial x} + \frac{\partial H}{\partial x} + I_{ex} = 0 \tag{12.1}$$

where H is the water level. As the explanation of the various physical quantities has already been provided, it is omitted here. The contribution of each term in the aforemen-

tioned equation was calculated for each ST measurement time, and the magnitudes were compared.

$\partial H/\partial x$ was obtained with the measured value of the water level of the ST. Other terms were obtained with the results of the hydraulic analysis, which is described in Section 4.1 in the main text. The time interval and spatial interval of the calculation were 1 min and 2 cm, respectively, which are the time resolutions and spatial resolutions of ST. The flow velocity and migrating speed of the y component under the experimental conditions were 10^{-4} to 10^{1} of the x components at any location regardless of the developmental state of the alternate bars. For simplicity, the y component is ignored in this section.

12.1.2 Verification Result

Figure 6.4 shows the time change of the box-beard diagram that displays the contribution of each term. This figure shows the (a) local term, (b) advection term, (c) pressure term, and (d) friction term, which correspond to the order of each term in Eq. (12.1). The figure shows that although the (b) advection term, (c) pressure term, and (d) friction term dominate the flow at any time, it can be confirmed that (a) the local term can be ignored because it is smaller than the aforementioned three terms. Even if the advection term with the smallest contribution in (b), (c), and (d) is compared with the local term, the contribution of the local term is 10^{-4} to 10^{-2} of the (b) advection term. In addition, it can be observed that the local term is extremely small. From this, it is inferred that it is physically appropriate to ignore the time gradient of flow in the alternate bars.

12.2 Appendix B：Derivation of the Two-Dimensional Equation of the Water Surface Profile

Appendix B presents the derivation processes of the two-dimensional equation of the water surface profile to derive the HPDE for the bed level. The governing equations used for the derivation consist of the following continuous equations and the equations of

motion. When deriving the equation, the flow can be treated as a pseudo-steady-state flow based on the verification results in Appendix B. Therefore, the following continuous equations and equations of motion were used for the derivation.

$$\frac{\partial[hu]}{\partial x} + \frac{\partial[hv]}{\partial y} = 0 \tag{12.2}$$

$$\frac{u}{g}\frac{\partial u}{\partial x} + \frac{v}{g}\frac{\partial u}{\partial y} + \frac{\partial z}{\partial x} + \frac{\partial h}{\partial x} + I_{ex} = 0 \tag{12.3}$$

$$\frac{u}{g}\frac{\partial v}{\partial x} + \frac{v}{g}\frac{\partial v}{\partial y} + \frac{\partial z}{\partial y} + \frac{\partial h}{\partial y} + I_{ey} = 0 \tag{12.4}$$

As an explanation of the various physical quantities has already been provided, it is omitted here.

The derivation of $\partial h/\partial x$ is described as follows. First, applying the product rule to Eq. (12.2) results in the following equation.

$$h\frac{\partial u}{\partial x} + u\frac{\partial h}{\partial x} + h\frac{\partial v}{\partial y} + v\frac{\partial h}{\partial y} = 0 \tag{12.5}$$

Next, for the first and third terms on the left side of Eq. (12.5),

$$u = \frac{1}{n}\frac{I_{ex}}{I_e^{1/2}}h^{2/3} \tag{12.6}$$

$$v = \frac{1}{n}\frac{I_{ey}}{I_e^{1/2}}h^{2/3} \tag{12.7}$$

$$\frac{\partial u}{\partial x} = \frac{\partial u}{\partial h}\frac{\partial h}{\partial x} + \frac{\partial u}{\partial I_{ex}}\frac{\partial I_{ex}}{\partial x} + \frac{\partial u}{\partial I_e}\frac{\partial I_e}{\partial x} = \frac{2}{3}\frac{u}{h}\frac{\partial h}{\partial x} + \frac{u}{I_{ex}}\frac{\partial I_{ex}}{\partial x} - \frac{1}{2}\frac{u}{I_e}\frac{\partial I_e}{\partial x} \tag{12.8}$$

$$\frac{\partial v}{\partial y} = \frac{\partial v}{\partial h}\frac{\partial h}{\partial y} + \frac{\partial v}{\partial I_{ey}}\frac{\partial I_{ey}}{\partial y} + \frac{\partial v}{\partial I_e}\frac{\partial I_e}{\partial y} = \frac{2}{3}\frac{v}{h}\frac{\partial h}{\partial y} + \frac{v}{I_{ey}}\frac{\partial I_{ey}}{\partial y} - \frac{1}{2}\frac{v}{I_e}\frac{\partial I_e}{\partial y} \tag{12.9}$$

After differentiating the composite function (Eq. (12.8) and Eq. (12.9)) using Manning's flow velocity formula (Eq. (12.6), Eq. (12.7)), substituting it into Eq. (12.5), and rearranging $\partial h/\partial x$, the following equation is obtained.

$$\frac{\partial h}{\partial x} = -\frac{3}{5}\frac{h}{I_{ex}}\frac{\partial I_{ex}}{\partial x} + \frac{3}{10}\frac{h}{I_e}\frac{\partial I_e}{\partial x} - \frac{v}{u}\frac{\partial h}{\partial y} - \frac{3}{5}\frac{vh}{uI_{ey}}\frac{\partial I_{ey}}{\partial y} + \frac{3}{10}\frac{vh}{uI_e}\frac{\partial I_e}{\partial y} \tag{12.10}$$

Next, after substituting Eq. (12.8) and the following Eq. (12.11) into the first and second terms of the equation of motion in the x direction for Eq. (12.3), we get

$$\frac{\partial u}{\partial y} = \frac{\partial u}{\partial h}\frac{\partial h}{\partial y} + \frac{\partial u}{\partial I_{ex}}\frac{\partial I_{ex}}{\partial y} + \frac{\partial u}{\partial I_e}\frac{\partial I_e}{\partial y} = \frac{2}{3}\frac{u}{h}\frac{\partial h}{\partial y} + \frac{u}{I_{ex}}\frac{\partial I_{ex}}{\partial y} - \frac{1}{2}\frac{u}{I_e}\frac{\partial I_e}{\partial y} \tag{12.11}$$

After substituting Eq. (12.10), which was organized earlier into Eq. (12.12), we get

$$\begin{aligned} &\frac{2}{3}\frac{u^2}{gh}\frac{\partial h}{\partial x} + \frac{u^2}{gI_{ex}}\frac{\partial I_{ex}}{\partial x} - \frac{1}{2}\frac{u^2}{gI_e}\frac{\partial I_e}{\partial x} + \frac{2}{3}\frac{uv}{gh}\frac{\partial h}{\partial y} \\ &+\frac{uv}{gI_{ex}}\frac{\partial I_{ex}}{\partial y} - \frac{1}{2}\frac{uv}{gI_e}\frac{\partial I_e}{\partial y} + \frac{\partial z}{\partial x} + \frac{\partial h}{\partial x} + I_{ex} = 0 \end{aligned} \tag{12.12}$$

The following equation can be obtained by rearranging $v/u\partial h/\partial y$.

$$\begin{aligned} \frac{v}{u}\frac{\partial h}{\partial y} &= \frac{3}{5I_{ex}}\left(\frac{u^2}{g} - h\right)\frac{\partial I_{ex}}{\partial x} + \frac{3}{10I_e}\left(-\frac{u^2}{g} + h\right)\frac{\partial I_e}{\partial x} \\ &+\frac{1}{5I_{ey}}\left(-\frac{2uv}{g} - \frac{3vh}{u}\right)\frac{\partial I_{ey}}{\partial y} + \frac{3}{10I_e}\left(-\frac{uv}{g} + \frac{vh}{u}\right)\frac{\partial I_e}{\partial y} + \frac{uv}{gI_{ex}}\frac{\partial I_{ex}}{\partial y} + \frac{\partial z}{\partial x} + I_{ex} \end{aligned} \tag{12.13}$$

After substituting Eq. (12.13) into Eq. (12.10) and rearranging it, the following $\partial h/\partial x$ is derived.

$$\frac{\partial h}{\partial x} = -\frac{\partial z}{\partial x} - I_{ex} - \frac{3}{5}\frac{u^2}{gI_{ex}}\frac{\partial I_{ex}}{\partial x} + \frac{3}{10}\frac{u^2}{gI_e}\frac{\partial I_e}{\partial x} + \frac{2}{5}\frac{uv}{gI_{ey}}\frac{\partial I_{ey}}{\partial y} + \frac{3}{10}\frac{uv}{gI_e}\frac{\partial I_e}{\partial y} - \frac{uv}{gI_{ex}}\frac{\partial I_{ex}}{\partial y} \tag{12.14}$$

By rearranging $\partial h/\partial y$ using the same process as before, the following equation for $\partial h/\partial y$ is obtained.

$$\frac{\partial h}{\partial y} = -\frac{\partial z}{\partial y} - I_{ey} - \frac{3}{5}\frac{v^2}{gI_{ey}}\frac{\partial I_{ey}}{\partial y} + \frac{3}{10}\frac{v^2}{gI_e}\frac{\partial I_e}{\partial y} + \frac{2}{5}\frac{uv}{gI_{ex}}\frac{\partial I_{ex}}{\partial x} + \frac{3}{10}\frac{uv}{gI_e}\frac{\partial I_e}{\partial x} - \frac{uv}{gI_{ey}}\frac{\partial I_{ey}}{\partial x} \tag{12.15}$$

13 Figure and Table

13.1 Table of Contents of Figures

Figures in Section 1

Figure 1.1 Aerial photos of the Chikuma river of Japan (a) before the flood, (b) after the flood (「Part 2 Chikumagawa teibou chousa iinnkai shiryou」(Ministry of Land, Infrastructure, Transport and Tourism) (https://www.hrr.mlit.go.jp/river/chikumagawateibouchousa/chikuma-02.pdf) created by processing).

Figure 1.2 Aerial photos of The fall of Ueda Bridge in Chikuma River of the Japan.

Figures in Section 2

Figure 2.1 Plan view of the experimental flume.

Figure 2.2 Temporal changes of the plan view in the observed bed topography.

Figure 2.3 Longitudinal view of the measured bed shape: (a) Initial stage of the experiment, (b) occurrence of alternate bars, (c) intermediate stage of the experiment, and (d) final stage of the experiment.

Figures in Section 3 None

Figures in Section 4

Figure 4.1 Temporal changes in the plan view for the observed water depth.

Figure 4.2 Difference between the measured and calculated values of the water depth that is made dimensionless using the measured value.

Figure 4.3 Temporal changes in the plan view for the calculated flow velocity.

Figure 4.4 Bed-level time waveform: (a) Left bank side, (b) center, (c) right bank side.

Figure 4.5 Temporal changes in the plan view for the observed bed topography and Δz_*.

13.2 Table of Contents of Tables

13.3 Figures

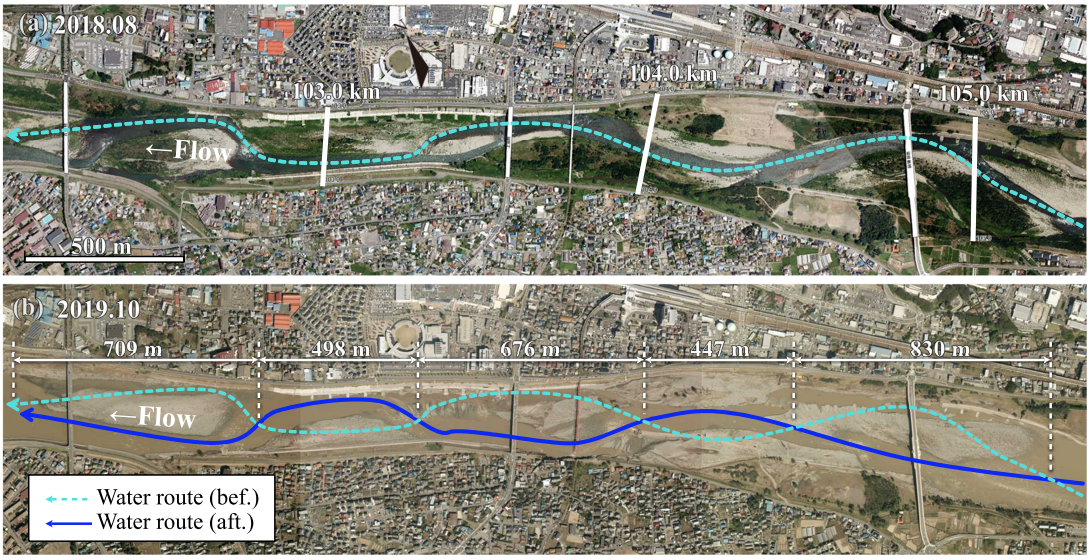

Figure 1.1: Aerial photos of the Chikuma river of Japan (a) before the flood, (b) after the flood (「Part 2 Chikumagawa teibou chousa iinnkai shiryou」(Ministry of Land, Infrastructure, Transport and Tourism) (https://www.hrr.mlit.go.jp/river/chikumagawateibouchousa/chikuma-02.pdf) created by processing).

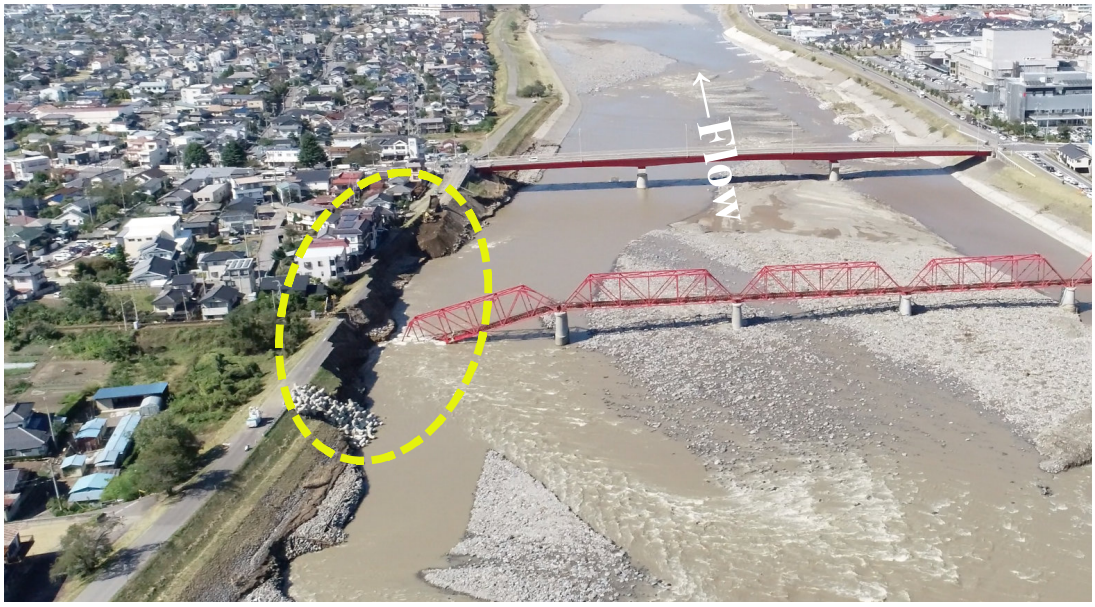

Figure 1.2: Aerial photos of The fall of Ueda Bridge in Chikuma River of the Japan

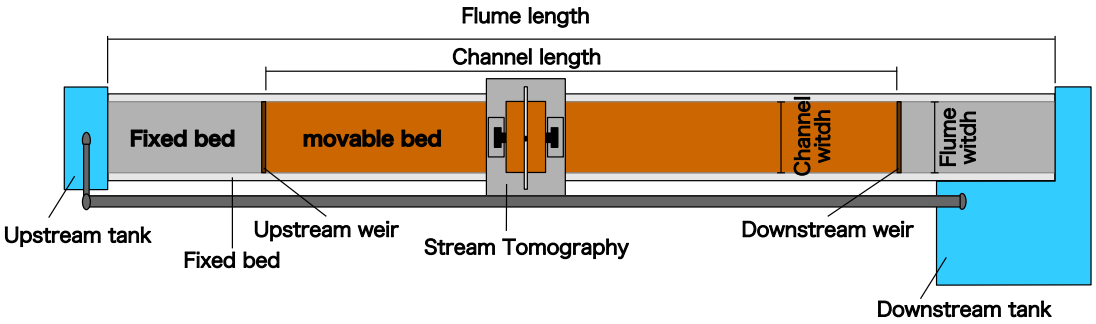

Figure 2.1: Plan view of the experimental flume.

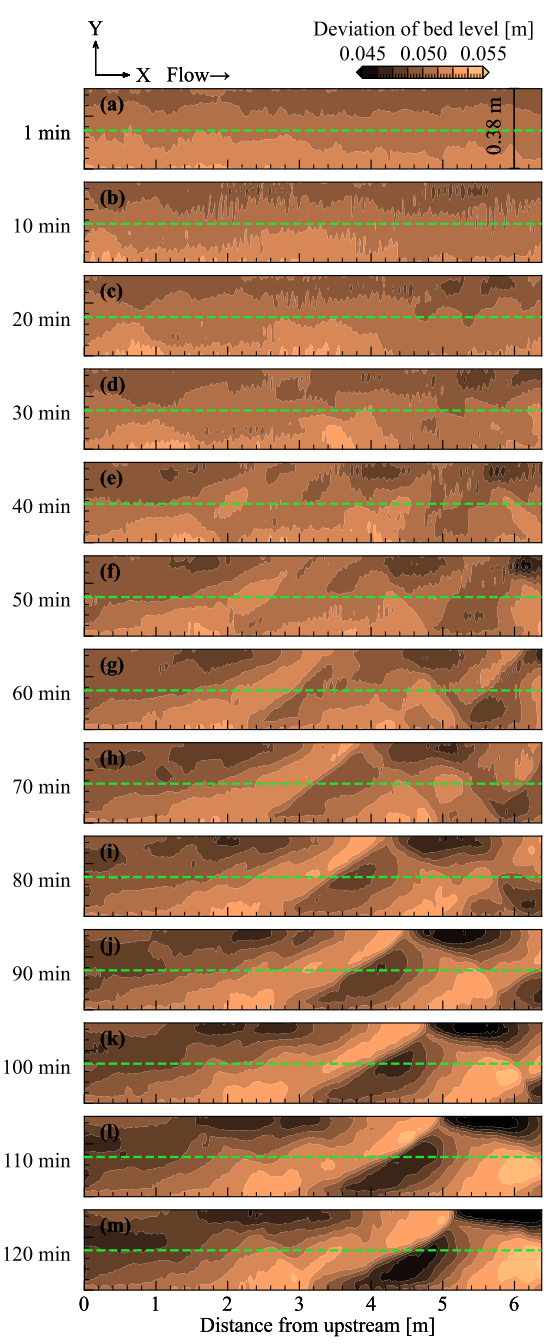

Figure 2.2: Temporal changes of the plan view in the observed bed topography.

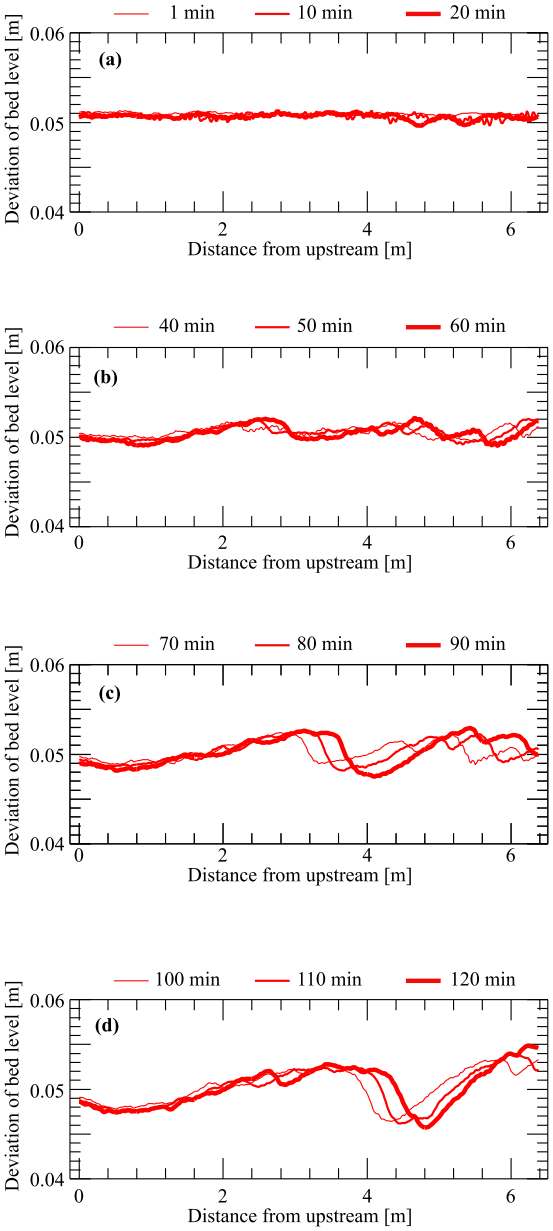

Figure 2.3: Longitudinal view of the measured bed shape: (a) Initial stage of the experiment, (b) occurrence of alternate bars, (c) intermediate stage of the experiment, and (d) final stage of the experiment.

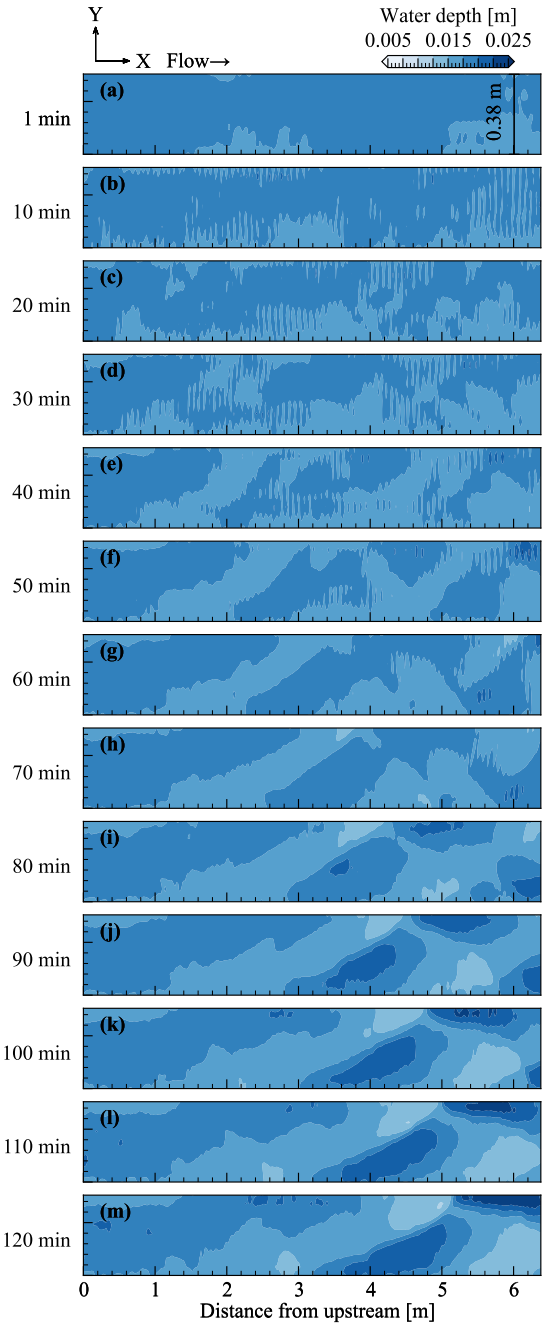

Figure 4.1: Temporal changes in the plan view for the observed water depth.

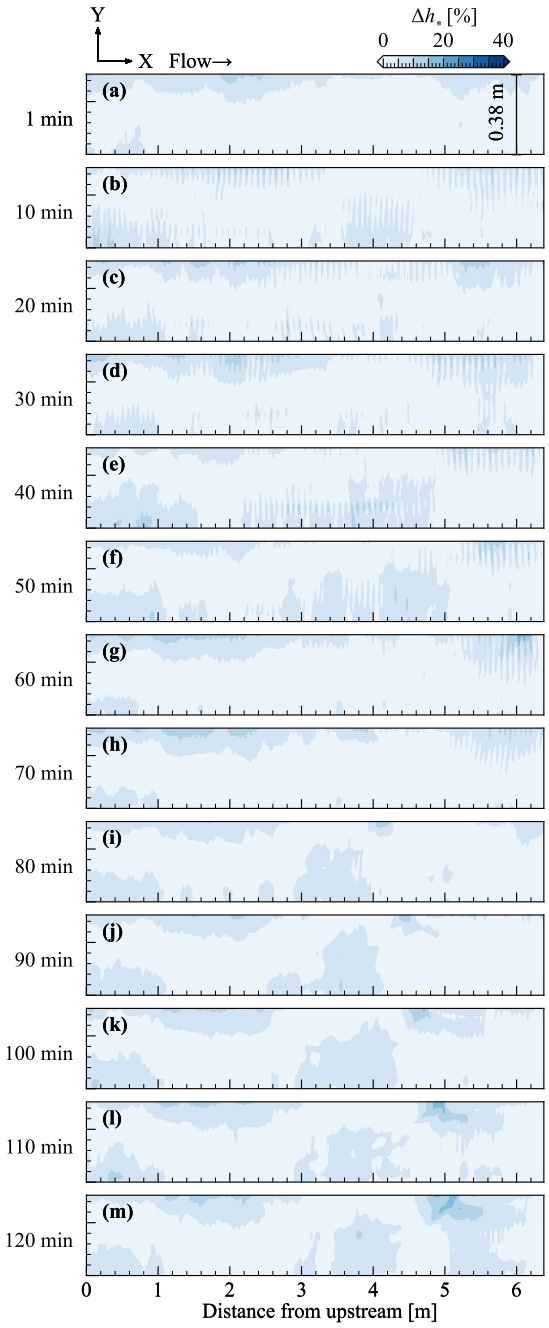

Figure 4.2: Difference between the measured and calculated values of the water depth that is made dimensionless using the measured value.

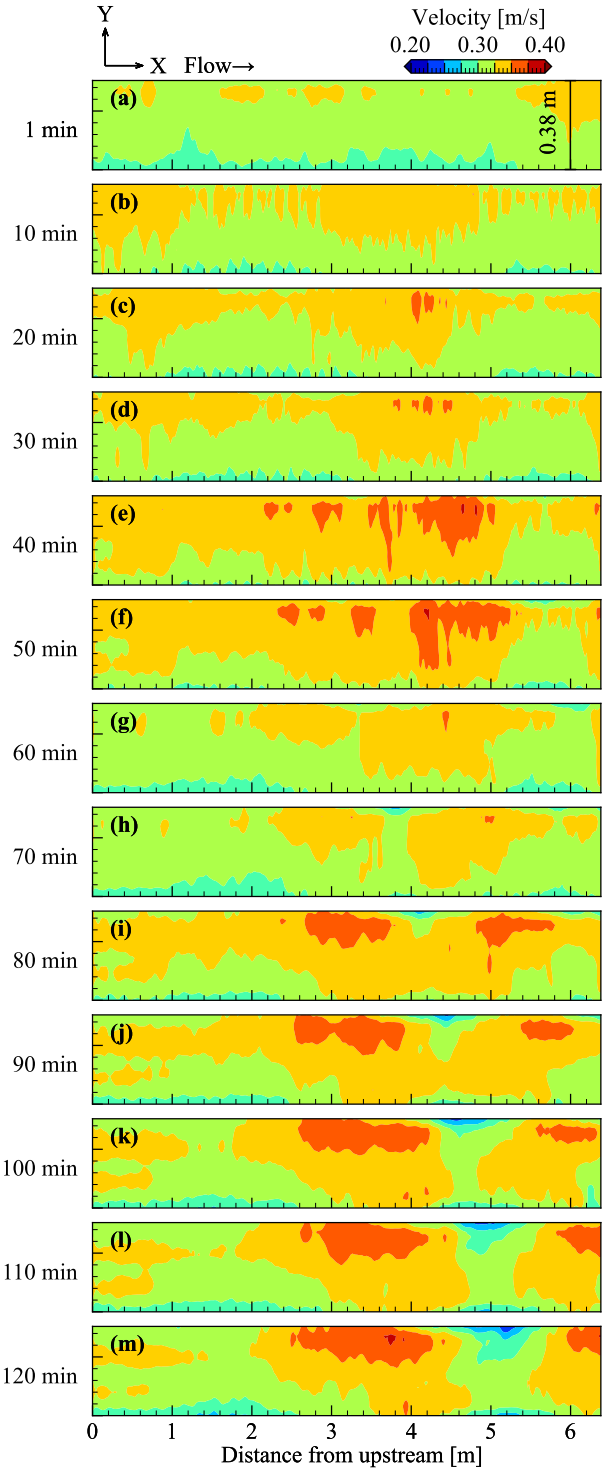

Figure 4.3: Temporal changes in the plan view for the calculated flow velocity.

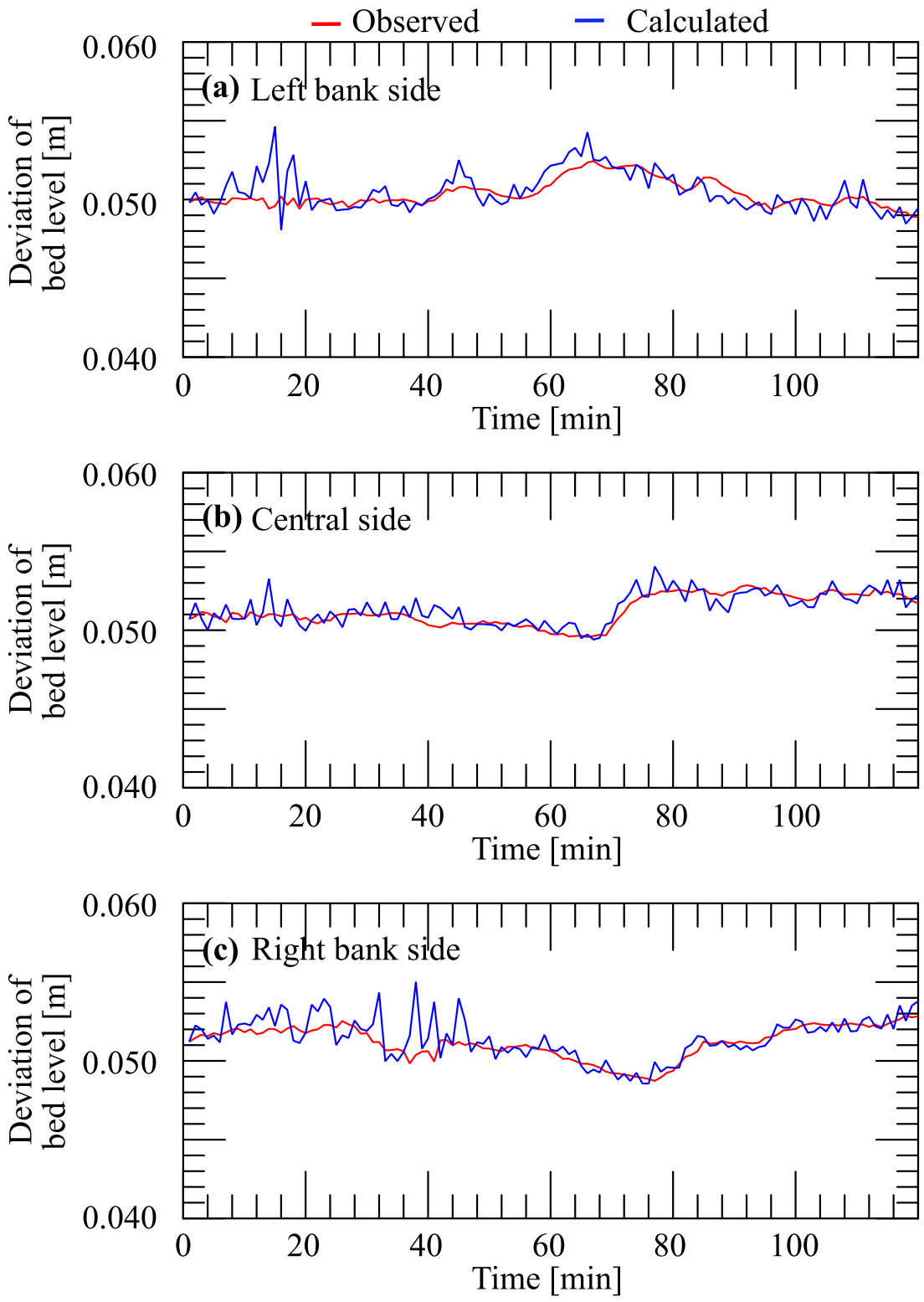

Figure 4.4: Bed-level time waveform: (a) Left bank side, (b) center, (c) right bank side.

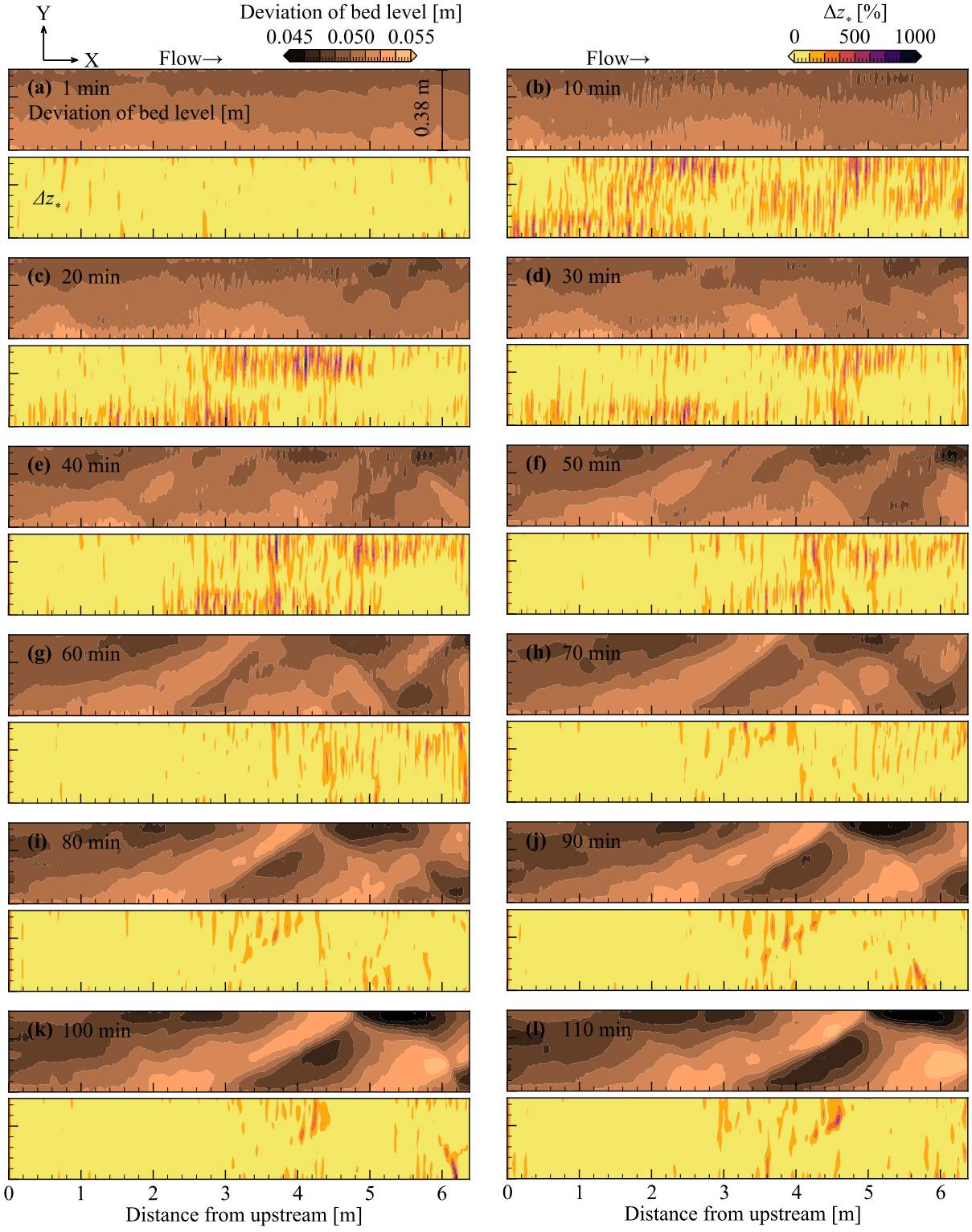

Figure 4.5: Temporal changes in the plan view for the observed bed topography and Δz_*.

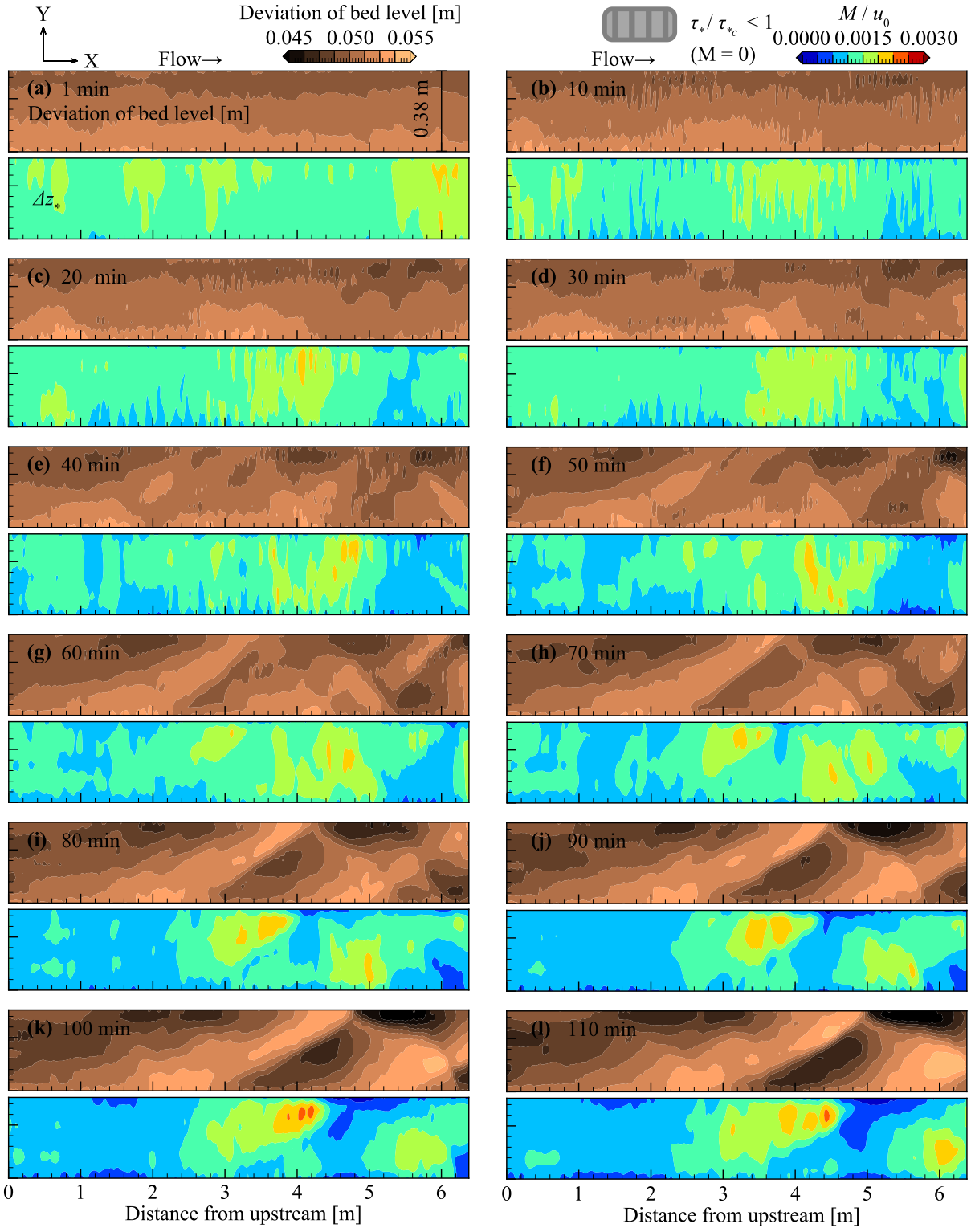

Figure 5.1: Temporal changes in the plan view for the observed bed topography and calculated migrating speed.

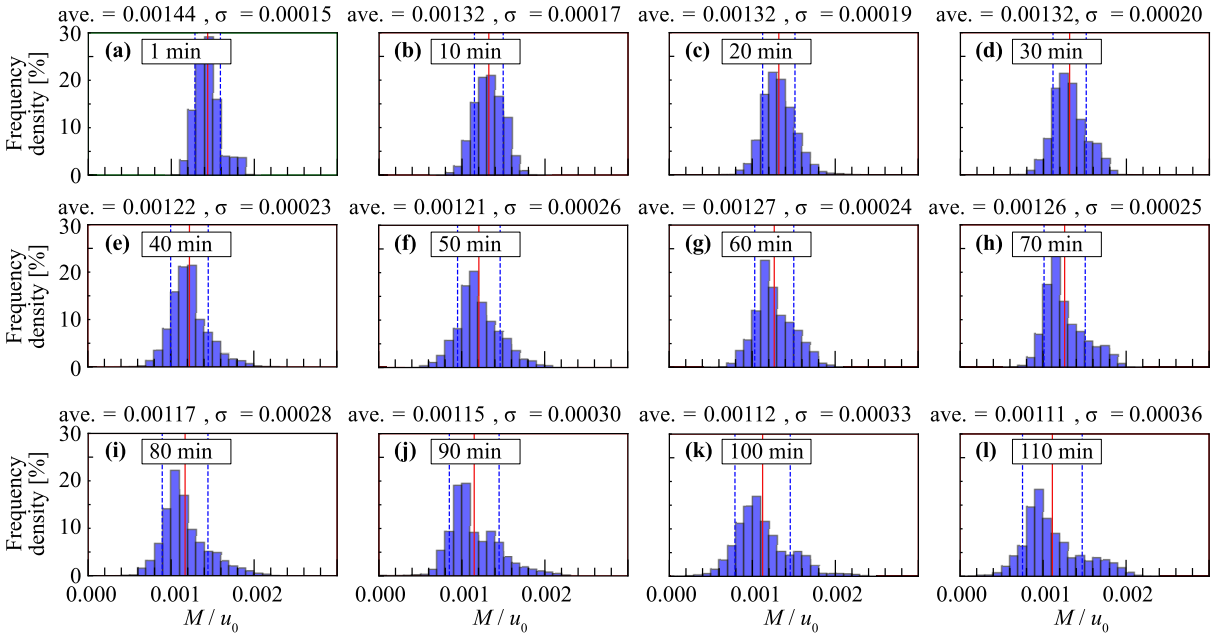

Figure 5.2: Histograms of migrating speed.

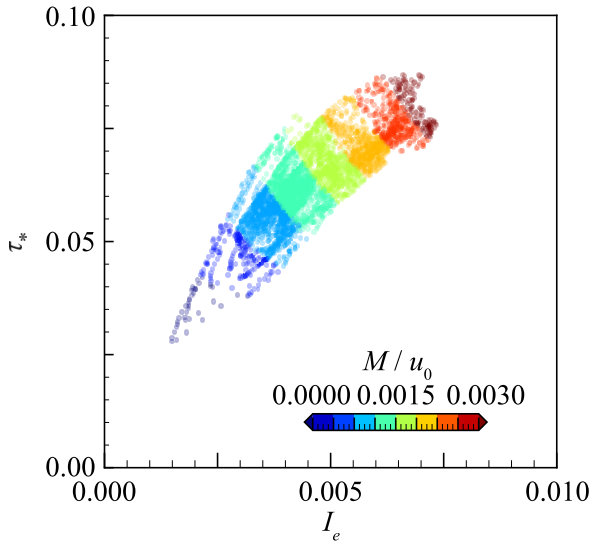

Figure 5.3: Relationship between energy slope, Shields number, and migrating speed.

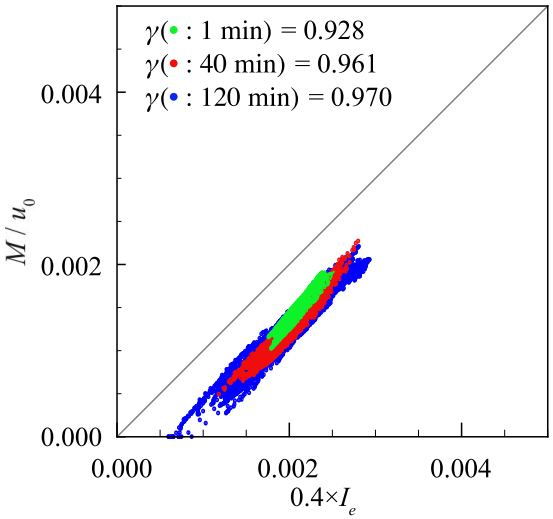

Figure 5.4: Relationship between migrating speed and energy slope.

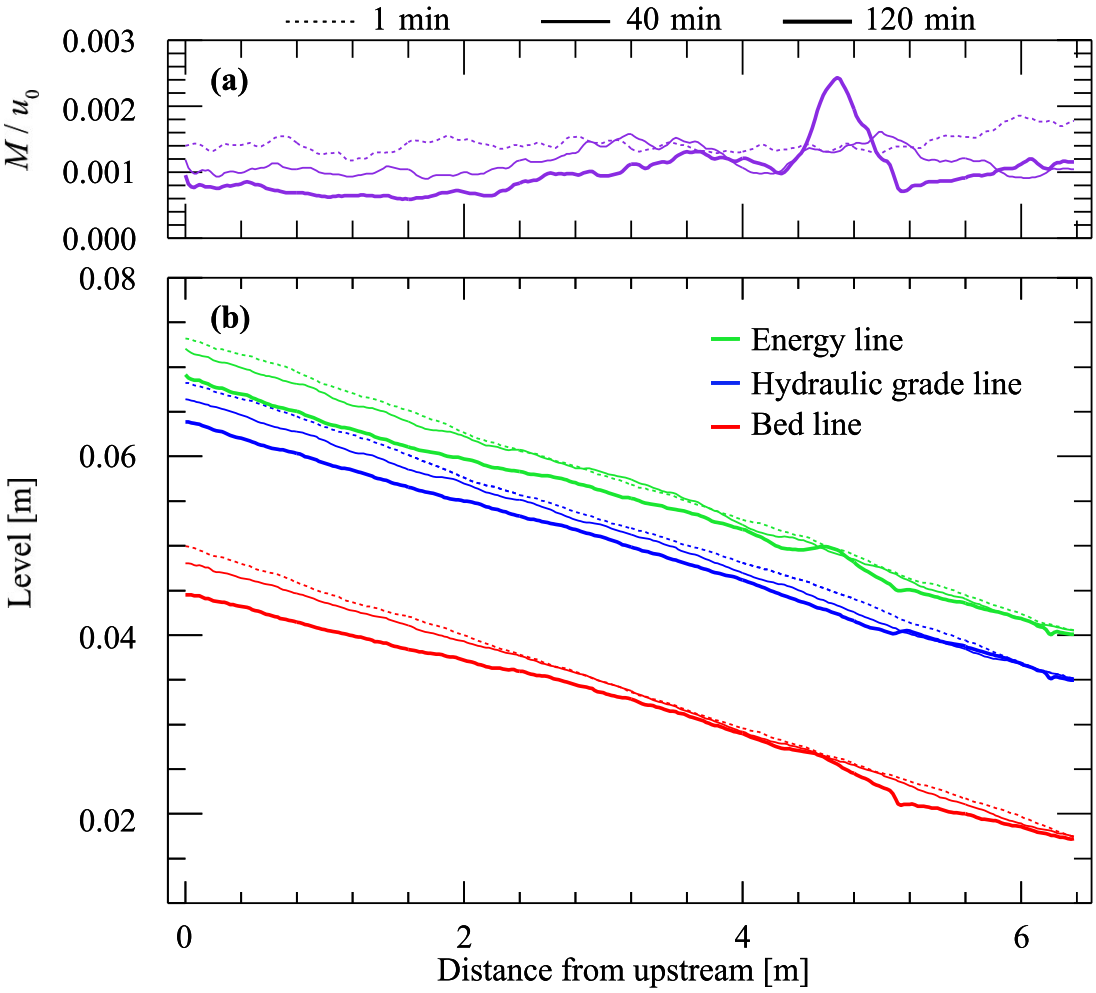

Figure 5.5: Longitudinal view of the (a) cross-sectional averaged migrating speed (b) and cross-sectional averaged bed level.

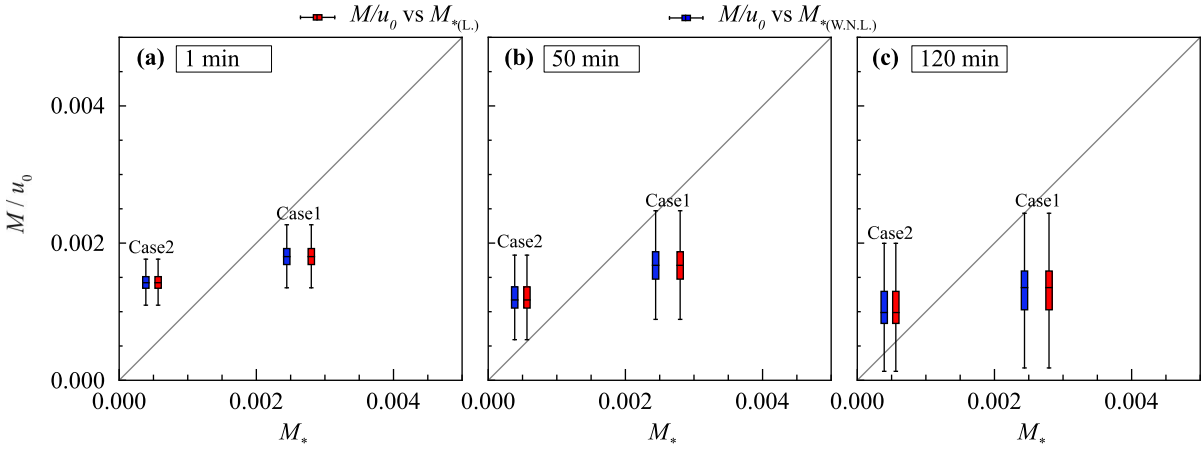

Figure 5.6: Relationship between migrating speed obtained by our method and migrating speed obtained by instability analysis.

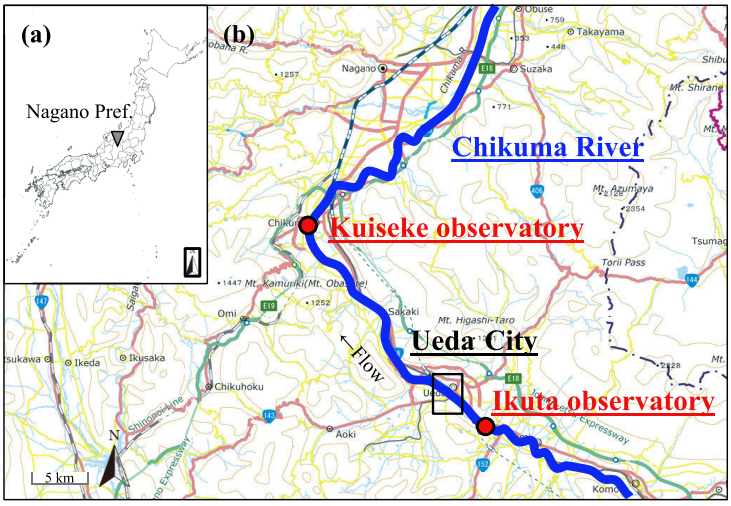

Figure 6.1: Overview of the study area: (a) geographic location, (b) map (GSI Maps (electronic land web) created by processing).

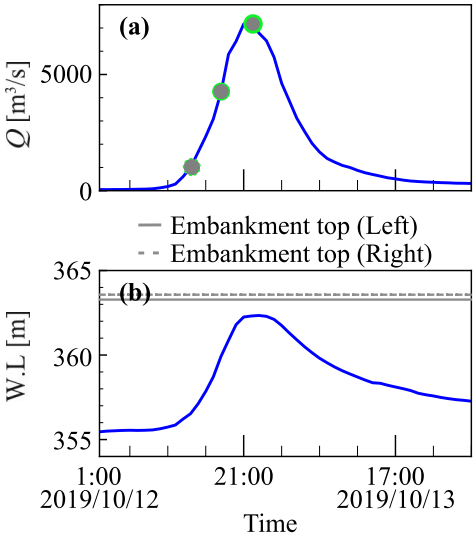

Figure 6.2: (a) Flow discharge hydrograph and (b) water level hydrograph.

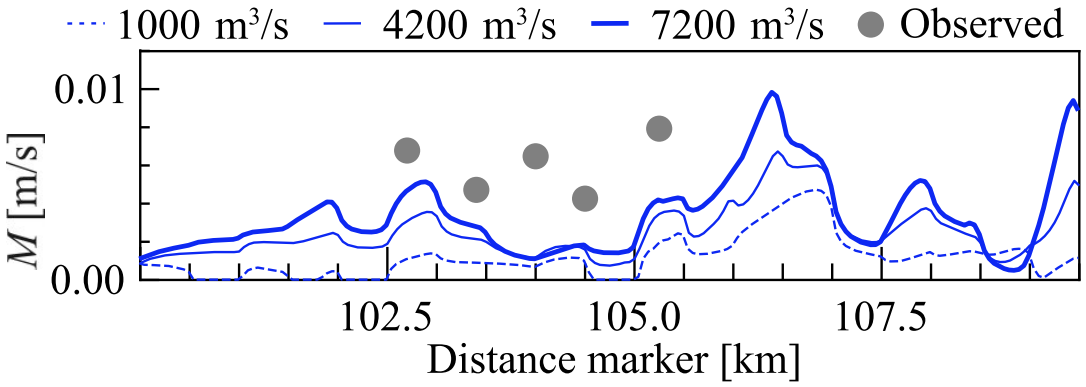

Figure 6.3: Calculated and measured values of migrating speed.

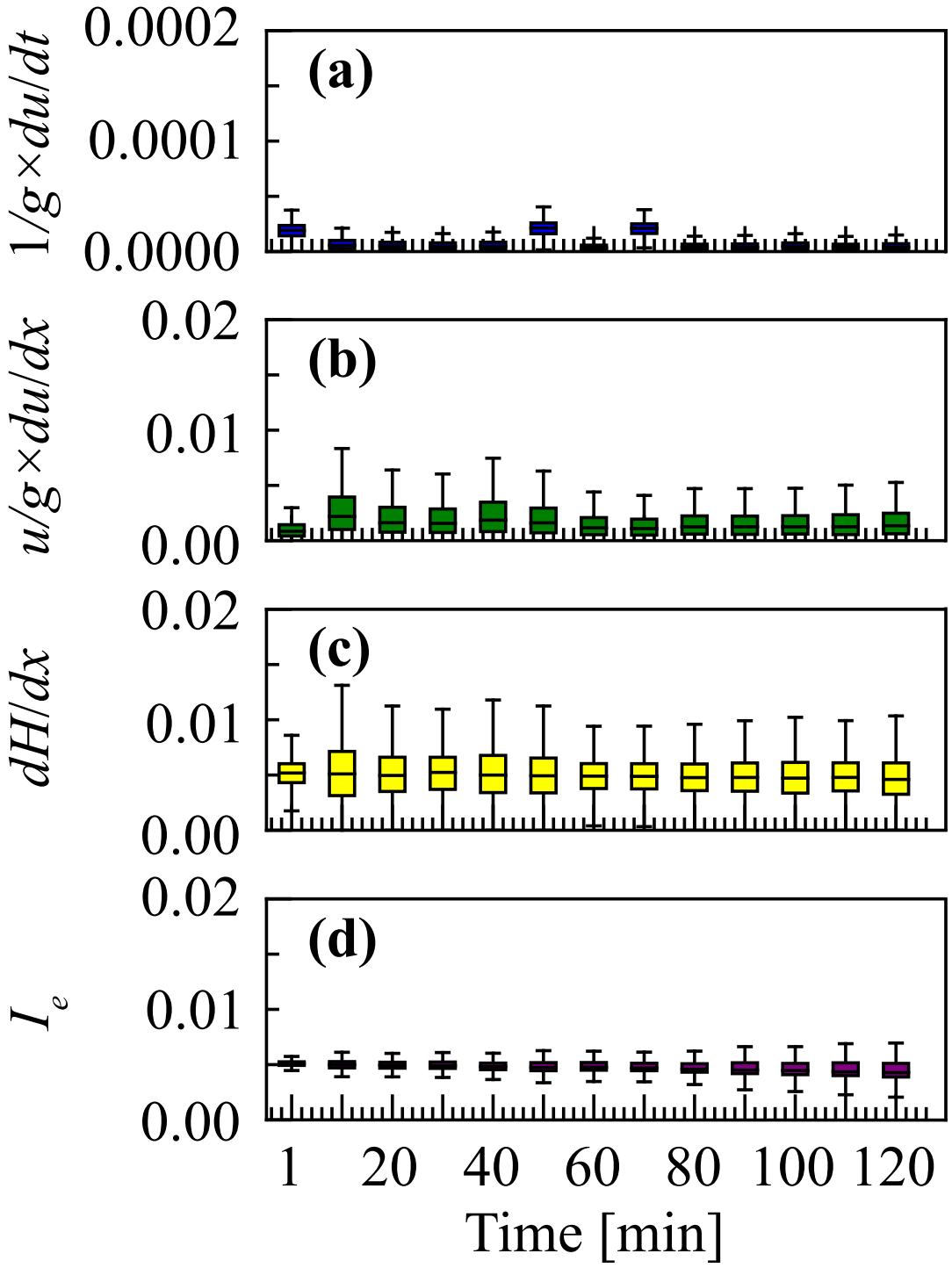

Figure 6.4: Temporal changes of the box plots for the (a) local term, (b) advection term, (c) pressure term, (d) and friction term.

13.4 Tables

Table 2.1: Experimental condition.

Case	Flow discharge [L/s]	width [m]	slope	h_0 [m]	$BI_0^{0.2}/h_0$	β	τ_*
1	2.0	0.45	1/160	0.014	11.4	31.45	0.0713
2	2.6	0.45	1/200	0.018	8.7	25.13	0.0714